Calhoun: The NPS Institutional Archive

DSpace Repository

Theses and Dissertations | 1. Thesis and Dissertation Collection, all items

2021-12

LONG-RANGE PREDICTION OF ATMOSPHERIC AND OCEANIC CONDITIONS AFFECTING NAVAL OPERATIONS IN THE SOUTH CHINA SEA (SCS)

Hardie, Matthew K.

Monterey, CA; Naval Postgraduate School

http://hdl.handle.net/10945/68722

This publication is a work of the U.S. Government as defined in Title 17, United States Code, Section 101. Copyright protection is not available for this work in the United States.

Downloaded from NPS Archive: Calhoun

http://www.nps.edu/library

Calhoun is the Naval Postgraduate School's public access digital repository for research materials and institutional publications created by the NPS community. Calhoun is named for Professor of Mathematics Guy K. Calhoun, NPS's first appointed -- and published -- scholarly author.

Dudley Knox Library / Naval Postgraduate School
411 Dyer Road / 1 University Circle
Monterey, California USA 93943

NAVAL POSTGRADUATE SCHOOL

MONTEREY, CALIFORNIA

THESIS

LONG-RANGE PREDICTION OF ATMOSPHERIC AND OCEANIC CONDITIONS AFFECTING NAVAL OPERATIONS IN THE SOUTH CHINA SEA (SCS)

by

Matthew K. Hardie

December 2021

Thesis Advisor: Tom Murphree
Co-Advisor: Megan Hutchins (FNMOC)

Approved for public release. Distribution is unlimited.

THIS PAGE INTENTIONALLY LEFT BLANK

REPORT DOCUMENTATION PAGE			*Form Approved OMB No. 0704-0188*

Public reporting burden for this collection of information is estimated to average 1 hour per response, including the time for reviewing instruction, searching existing data sources, gathering and maintaining the data needed, and completing and reviewing the collection of information. Send comments regarding this burden estimate or any other aspect of this collection of information, including suggestions for reducing this burden, to Washington headquarters Services, Directorate for Information Operations and Reports, 1215 Jefferson Davis Highway, Suite 1204, Arlington, VA 22202-4302, and to the Office of Management and Budget, Paperwork Reduction Project (0704-0188) Washington, DC 20503.

1. AGENCY USE ONLY *(Leave blank)*	**2. REPORT DATE** December 2021	**3. REPORT TYPE AND DATES COVERED** Master's thesis

4. TITLE AND SUBTITLE
LONG-RANGE PREDICTION OF ATMOSPHERIC AND OCEANIC CONDITIONS AFFECTING NAVAL OPERATIONS IN THE SOUTH CHINA SEA (SCS)

5. FUNDING NUMBERS

6. AUTHOR(S) Matthew K. Hardie

7. PERFORMING ORGANIZATION NAME(S) AND ADDRESS(ES)
Naval Postgraduate School
Monterey, CA 93943-5000

8. PERFORMING ORGANIZATION REPORT NUMBER

9. SPONSORING / MONITORING AGENCY NAME(S) AND ADDRESS(ES)
N/A

10. SPONSORING / MONITORING AGENCY REPORT NUMBER

11. SUPPLEMENTARY NOTES The views expressed in this thesis are those of the author and do not reflect the official policy or position of the Department of Defense or the U.S. Government.

12a. DISTRIBUTION / AVAILABILITY STATEMENT
Approved for public release. Distribution is unlimited.

12b. DISTRIBUTION CODE
A

13. ABSTRACT (maximum 200 words)

During each winter, the South China Sea (SCS) experiences strong northerly winds associated with the East Asian winter monsoon (EAWM). However, the intensity of the winds varies from year to year. In our study, we investigated the regional and global scale oceanic and atmospheric factors that trigger and contribute to these wind variations in the SCS. We found that SST anomalies in the equatorial Pacific and SLP anomalies along coastal China and the Maritime Continent are major contributors to SCS winds. We also determined how wind variations in the SCS influence oceanic and atmospheric variables relevant to the U.S. Navy. We then developed and tested two long-range forecasting methods to predict the SCS wind variations at subseasonal to seasonal (S2S) lead times. We determined that both methods show high forecasting skill at two- to five-month time leads, which greatly improves long-range planning for operations in the SCS. Furthermore, we analyzed the influence of climate change on cool and warm events in the SCS (e.g., their intensity and frequency.) We determined that the overall strength of the northerly winds in the SCS has decreased over the past 52 years.

14. SUBJECT TERMS South China Sea, SCS, winter, East Asian winter monsoon, EAWM, northerly winds, cool events, warm events, subseasonal to seasonal, S2S	**15. NUMBER OF PAGES** 109
	16. PRICE CODE

17. SECURITY CLASSIFICATION OF REPORT	**18. SECURITY CLASSIFICATION OF THIS PAGE**	**19. SECURITY CLASSIFICATION OF ABSTRACT**	**20. LIMITATION OF ABSTRACT**
Unclassified	Unclassified	Unclassified	UU

NSN 7540-01-280-5500

Standard Form 298 (Rev. 2-89)
Prescribed by ANSI Std. 239-18

THIS PAGE INTENTIONALLY LEFT BLANK

Approved for public release. Distribution is unlimited.

LONG-RANGE PREDICTION OF ATMOSPHERIC AND OCEANIC CONDITIONS AFFECTING NAVAL OPERATIONS IN THE SOUTH CHINA SEA (SCS)

Matthew K. Hardie
Lieutenant Commander, United States Navy
BS, United States Naval Academy, 2012

Submitted in partial fulfillment of the
requirements for the degree of

MASTER OF SCIENCE IN METEOROLOGY AND PHYSICAL OCEANOGRAPHY

from the

NAVAL POSTGRADUATE SCHOOL
December 2021

Approved by: Tom Murphree
Advisor

Megan Hutchins
Co-Advisor

Wendell A. Nuss
Chair, Department of Meteorology

THIS PAGE INTENTIONALLY LEFT BLANK

ABSTRACT

During each winter, the South China Sea (SCS) experiences strong northerly winds associated with the East Asian winter monsoon (EAWM). However, the intensity of the winds varies from year to year. In our study, we investigated the regional and global scale oceanic and atmospheric factors that trigger and contribute to these wind variations in the SCS. We found that SST anomalies in the equatorial Pacific and SLP anomalies along coastal China and the Maritime Continent are major contributors to SCS winds. We also determined how wind variations in the SCS influence oceanic and atmospheric variables relevant to the U.S. Navy. We then developed and tested two long-range forecasting methods to predict the SCS wind variations at subseasonal to seasonal (S2S) lead times. We determined that both methods show high forecasting skill at two- to five-month time leads, which greatly improves long-range planning for operations in the SCS. Furthermore, we analyzed the influence of climate change on cool and warm events in the SCS (e.g., their intensity and frequency.) We determined that the overall strength of the northerly winds in the SCS has decreased over the past 52 years.

THIS PAGE INTENTIONALLY LEFT BLANK

TABLE OF CONTENTS

LIST OF FIGURES

THIS PAGE INTENTIONALLY LEFT BLANK

LIST OF TABLES

LIST OF ACRONYMS AND ABBREVIATIONS

ACAF	Advanced Climate Analysis of Forecasting
AL	Aleutian low
AN	above normal
AO	Arctic Oscillation
ASO	August, September, October
ASW	anti-submarine warfare
BN	below normal
CFR	Council on Foreign Relations
CFSR	climate forecast system reanalysis
CSIS	Center for Strategic and International Studies
CPC	climate prediction center
CS	Coral Sea
CTP	Central Tropical Pacific
DJF	December, January, February
DOD	Department of Defense
EAWM	East Asian winter monsoon
ECS	East China Sea
EDH	evaporation duct height
EM	Electromagnetic
EN	El Niño
ENLN	El Niño La Niña
ESPC	Earth System Prediction Capability
FAR	false alarm ratio
ft	Feet
FNMOC	Fleet Numerical and Oceanography Center
FONOP	freedom of navigation operation
g	Grams
g/kg	grams per kilogram
HR	hit rate
HSS	Heidke Skill Score

ISR	intelligence, surveillance, and reconnaissance
JAS	July, August, September
K	Kelvin
kg	Kilogram
LN	La Niña
LTM	long term mean
LR	linear regression
LRF	long range forecasting
mb	millibar
MC	Maritime Continent
MLR	multiple linear regression
m/s	meters per second
NAO	North Atlantic Oscillation
NDJ	November, December, January
NN	near normal
NOAA	National Oceanic and Atmospheric Administration
NPH	North Pacific High
NRL	U.S. Naval Research Laboratory
NWS	National Weather Service
OLR	outgoing longwave radiation
OLRA	outgoing longwave radiation anomaly
OND	October, November, December
ONI	Oceanic Niño Index
PC	percent correct
PNA	Pacific North American index
PRC	People's Republic of China
PSL	Physical Science Division
R	correlation coefficient
S2S	subseasonal to seasonal
SCS	South China Sea
SLD	sonic layer depth
SLP	sea level pressure

SLR	simple linear regression
SLPA	sea level pressure anomaly
SH	Siberian High
SON	September, October, November
SST	sea surface temperature
SSTA	sea surface temperature anomaly
SWH	significant wave height
TCN	Traditional Climate Normal
TL	tropical low
v	meridional winds
WIO	Western Indian Ocean
WNP	Western north Pacific
WW3	Wave Watch III
ZA	geopotential height anomalies

THIS PAGE INTENTIONALLY LEFT BLANK

ACKNOWLEDGMENTS

I would like to thank my advisor, Professor Tom Murphree, for the guidance, mentorship, and motivation throughout the entire thesis process. Without Tom, I would not have been able to pursue my interest in climatology and long-range forecasting. The past few years were challenging and unprecedented for the entire NPS community. Tom remained steadfast and encouraging throughout the entire research process, all while juggling working from a home environment and a global pandemic. Tom's dedication to science and climate expertise are invaluable assets for the entire NPS METOC community. All students who have Tom as an instructor will leave NPS with a better understanding and appreciation of Earth's climate system.

I would also like to thank the other professors and military leadership within the METOC program. Their ability to flex during the COVID-19 pandemic allowed my cohort to continue our studies in a safe and effective manner. I hope that NPS does not have to deal with another pandemic for some time, but if it does, I know the faculty will be able to push forward and shine brightly yet again.

I could not have made it through these last few years at NPS without the help of everyone in my cohort. I think it's fair to say that we had the most unique NPS experience ever. I can't thank them enough for their friendship, brilliance, and laughs over the past few years. I'm honored to be a part of this incredible group of officers, and I look forward to working together for the rest of our careers.

And last but not least, I'd like to thank my family who supported me during my tour here at NPS. To my wife, Colleen, thank you for your dedication to our children and your infectious enthusiasm. Your support means the world to me, and I look forward to starting our next chapter in life after NPS.

THIS PAGE INTENTIONALLY LEFT BLANK

I. INTRODUCTION

A. BACKGROUND AND MOTIVATION

The South China Sea (SCS) has a complicated history regarding territorial claims that date back more than half a century. The People's Republic of China (PRC) implements a "nine-dash line that encompasses most of the water in the South China Sea" (Office of the Secretary of Defense 2017). This line remains vague and unambiguous. Other countries in the region, like Vietnam, Malaysia, Brunei, the Philippines, and Taiwan, all claim areas of the SCS. Figure 1 depicts the Indo-Pacific region and includes the "nine-dash line."

The white box corresponds to the SCS (Coordinates 8–18°N, 110–120°E).

Figure 1. Map of the Indo-Pacific region. Source: The Nations Online Project at nationsonline.org.

Natural resources within the SCS provide ample motivation for the surrounding countries. The Council on Foreign Relations (CFR) found that the SCS has an estimated "11 million billion barrels of untapped oil and 190 trillion cubic feet of natural gas" (CFR 2021). In addition to the resources, establishing land-based claims allows for control of activity in the area. According to the Center for Strategic and International Studies (CSIS), $3.37 trillion in total trade passed through the SCS in 2016 alone (China Power Project 2017). Over the past few years, the PRC has also steadily expanded its military expansion into the SCS by building multiple islands with runways, bases, and ports.

The PRC's excessive territorial claims and misinterpretation of international law have become one of the most important U.S. Department of Defense (DOD) policies. In the 2018 National Defense Strategy, James Mattis emphasized the importance of the SCS early in the document's introduction. Mattis stated that "China is a strategic competitor using predatory economics to intimidate its neighbors while militarizing features in the South China Sea" (Mattis 2018). To curb the PRC's influence, the U.S. Navy has conducted many freedom of navigation operations (FONOPs) (USNI 2018) and military exercises within the SCS (CNN 2021). The PRC continues to denounce the U.S. actions within the area, and as of late 2021, there appears to be no end in sight for a peaceful compromise between any nations involved.

Knowing that the SCS will remain a highly contested body of water for at least the near future, U.S. Navy planners would benefit significantly from improved long-range forecasting within the area of operations. A yearly winter (November-March) phenomenon, known as the East Asian winter monsoon (EAWM), brings strong northerly winds, cold temperatures, and wintery precipitation throughout the East Asian region, especially down through the SCS. The EAWM, and other monsoons around the world, have been the topic of scientific research for over 350 years (Wang 2007). Figure 2 shows the 1000 mb meridional (v) winds for the SCS winters from 1969–2021. All years feature negative v wind values, meaning winds from the north (northerly winds). The strongest v wind values occur during the middle of the winter season during the months of December, January, and February (DJF).

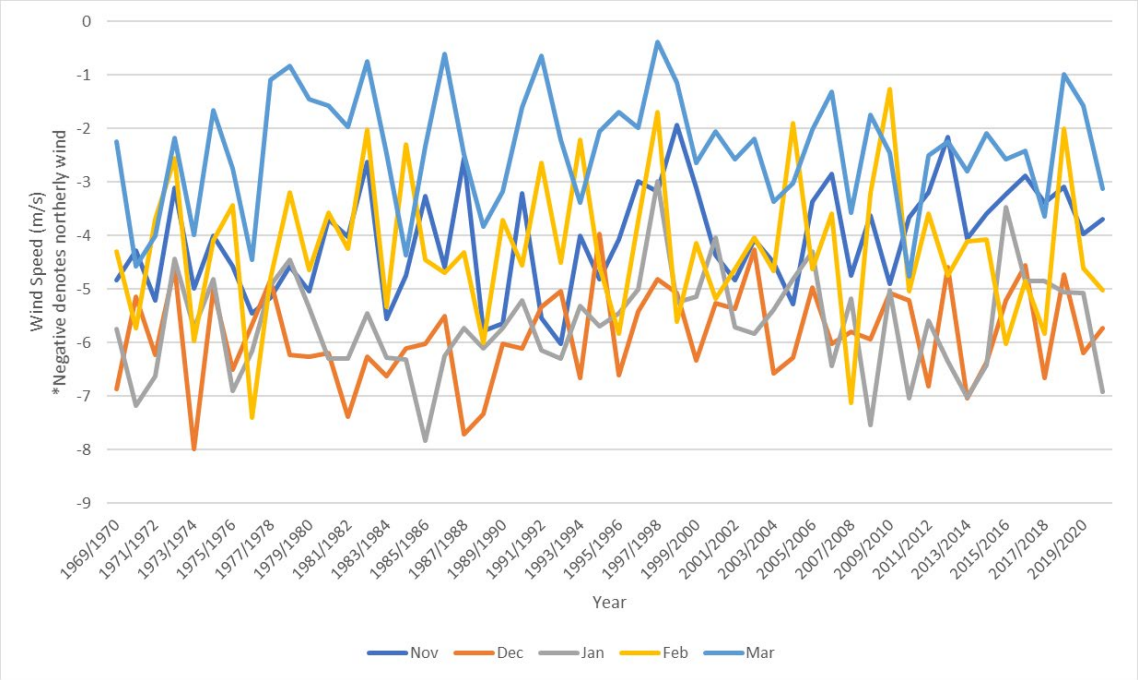

Figure 2. Timeseries of SCS 1000 mb meridional wind (m/s) for the winter months of Nov–Mar from 1969–2021.

In this research, we created several figures using the data access and product generation sites provided by the National Oceanic and Atmospheric Administration (NOAA)/ Earth Systems Research Laboratory (ESRL)'s Physical Science Division (PSL), Boulder, Colorado. These sites are accessible at: http://psl.noaa.gov/. Figure 3, which is explained below, is an example of one of these figures. Other examples are identified by the statement: "PSL based figure" in the figure captions.

Figure 3 is a visual representation of the averaged 1000 mb vector winds from 1981–2010, which is the current reference, or Traditional Climate Normal (TCN), base period for calculating climate normals. The 30-year period is often called climatology, or the long term mean (LTM). The predominant wind direction is from the northeast and the winds extend from the northern latitudes over Siberia to the Equator. The maximum averaged wind speed approaches 10 m/s in the southern portion of the SCS.

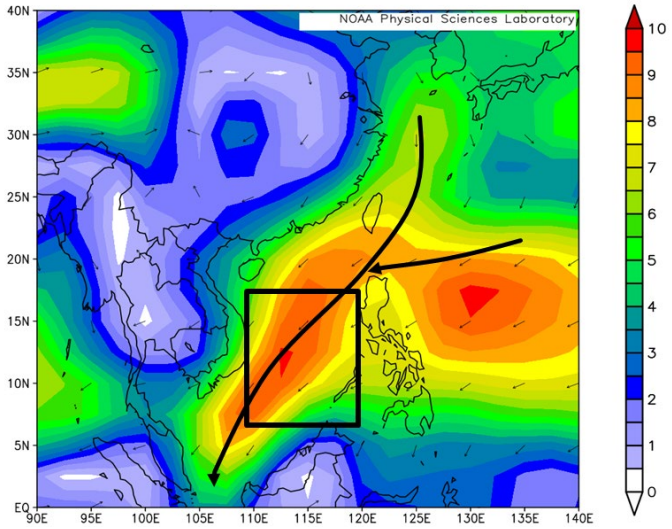

The black box corresponds to the SCS (Coordinates 8–18°N, 110–120°E). The black arrows correspond to the average overall meridional flow through the SCS region. PSL based figure.

Figure 3. DJF 1000 mb vector winds (m/s) long term mean (LTM)

Periods when the EAWM is particularly strong can cause major disruptions to naval operations, such as the inability of ships to operate in the area due to high seas and grounding of flight operations. Periods of when the EAWM is particularly weak are nearly as important as the strong periods. A relaxation of the northerly winds could allow naval planners to exercise in the area when other nations consider the area too harsh to operate. Before the prediction of the EAWM can be studied, the basics of the EAWM must be known and understood. Figure 4 shows the sea level pressures (SLP) LTM. Four major semipermanent pressure systems, the Siberian High (SH), the Aleutian Low (AL), North Pacific High (NPH), and Tropical Low (TL), all work together to produce the winds discussed in Figure 3. Of the four major pressure centers, the SH is the most important driver of the EAWM (Chan and Li 2004).

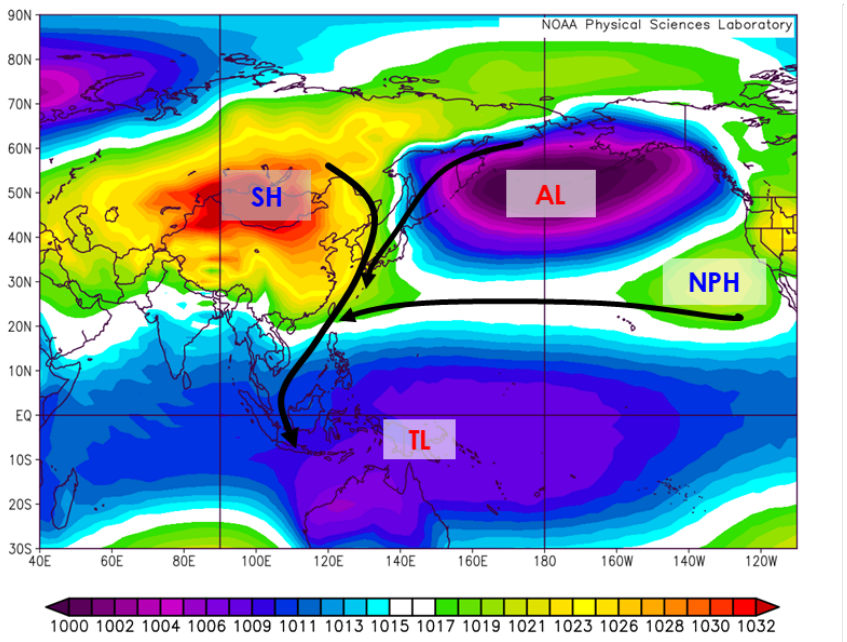

The black arrows in this figure correspond to the overall flow contributing to the flow through the SCS. The SH is the Siberian High, AL is the Aleutian Low, NPH is the North Pacific High, and TL is the Tropical Low. PSL based figure.

Figure 4. DJF sea level pressures (SLP) long term mean (LTM)

Chan and Li (2004) states "the EAWM results from the development of a cold-core high over the Siberia-Mongolia region. The movement of this cold air southward, apparently related to the polar and subtropical jet streams, produces pressure surges and temperature drops across the Asian continent" (Chan and Li 2004). Although the EAWM would not exist without the SH, it is also important to look at the three other major pressure centers in the Pacific Ocean to fully understand the EAWM. The strength of the AL brings more cold air from the Arctic region westward, where the air meets with the descending Siberian air. The NPH, although thousands of miles away off the coast of California, also brings air from across the Pacific Ocean, where it joins the southward moving cold air. All this air then flows south into the TL located over the Maritime Continent (MC) region. The location and strength of the pressure gradient between the Asian continent and MC change throughout the season.

There are periods during the winter season where the EAWM is especially strong. These synoptic events, known as cold surges, occur approximately ten times every winter (Chen et al. 2004). They bring brutally cold temperatures, high winds, and winter precipitation over the course of a few days. Figure 5 shows an example of a cold surge that occurred from 28 Dec 2020 through 31 Dec 2020. Averaged v winds over the four day period was about 8 m/s from the East China Sea (ECS) through the SCS, as indicated by the black circle on the upper right panel. When compared to the LTM, those winds over that four day period were approximately 4 m/s stronger than normal, as indicated by the black circle on the bottom right panel. Conducting naval operations during cold surges can be extremely dangerous due to the high winds and seas. Naval ships have certain limitations on wave heights and cannot operate when the seas are too high. It is for this reason that the U.S. Navy tends to avoid the SCS during the winter months. However, if the strength of the EAWM and subsequent cold surges can be predicted at long time leads (2 weeks to a few months), the U.S. Navy planners would have an advantage over SCS operations if tensions continue to escalate.

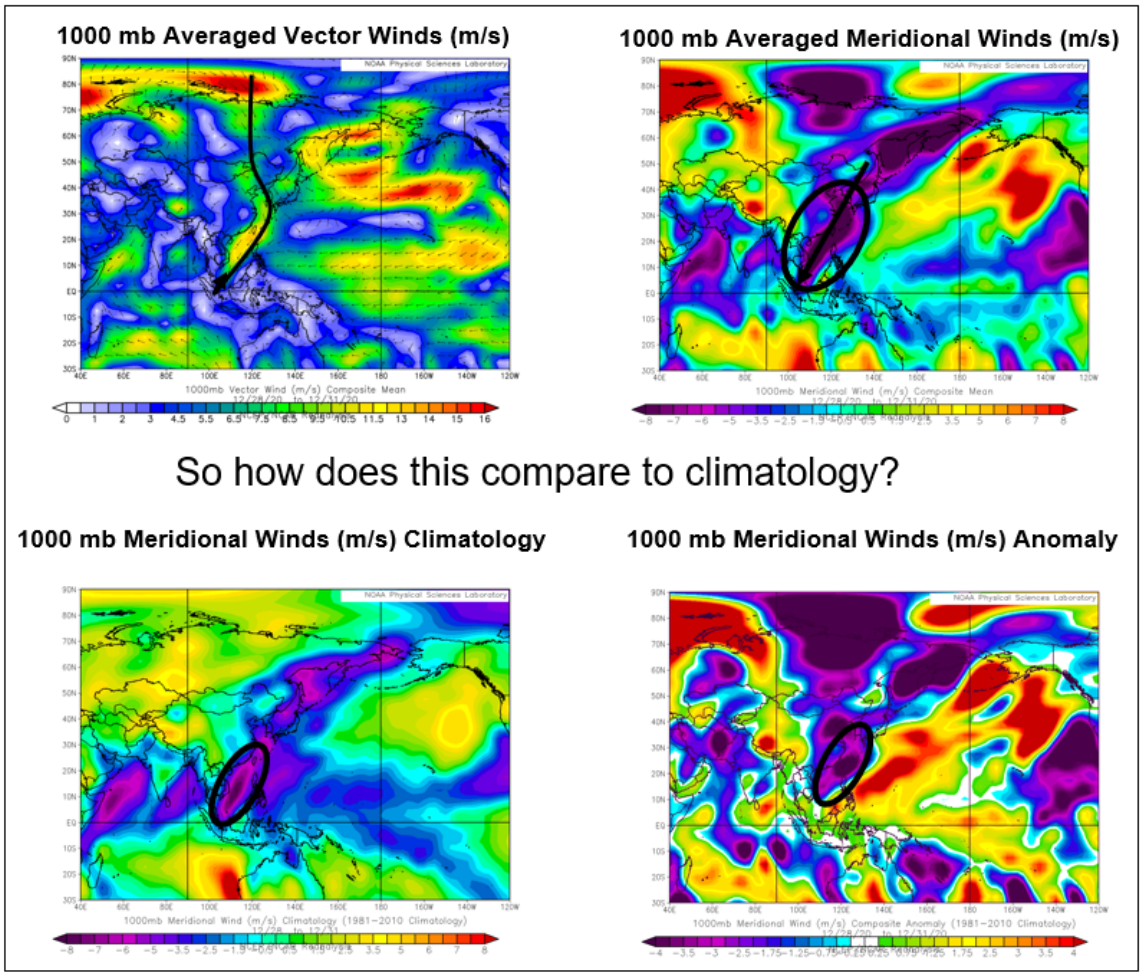

The upper left panel of this figure shows the 1000 mb averaged vector winds (m/s) for the 28–31 Dec cold surge event. The upper right figure shows the 1000 mb averaged meridional winds (m/s) for the 28–31 cold surge event. The bottom left panel shows the LTM meridional winds. The bottom right panel shows the difference between the cold surge event and LTM, or the anomaly. The black arrows are drawn to show the overall flow. The black circles denote our area of interest. PSL based figure.

Figure 5. An example of a cold surge from 28 Dec 2020–31 Dec 2020.

B. CURRENT METOC SUPPORT TO SCS DEPLOYERS

Most of the pre-deployment long-range forecast material for the Navy is provided by the Fleet Numerical Meteorology and Oceanography Center (FNMOC) (Ilczuk 2016). FNMOC's climate division maintains a climatology portion of FNMOCs website to include static/pre-made briefs pertaining to certain geographical areas of the world as well as the Advanced Climate Analysis of Forecasting (ACAF) tool. ACAF provides users with

a hands-on option to create climate products using various analysis and reanalysis data sets. Users have a variety of variables to chose from to include air temperature, winds, and geopotential heights. ACAF utilizes the Climate Forecast System Reanalysis (CFSR) for specific atmospheric and oceanic variables for certain areas of the world (Saha et al. 2010). ACAF also provides reanalysis for wave variables like significant wave height, mean wave direction, and mean wave period through the NAVO Wave Watch III (WW3) dataset (Swail et al. 2006).

Although FNMOC's climate division provides extremely useful support products that can be used in long-range planning, FNMOC currently does not have a trusted long-range forecasting ability to provide to the fleet. Subseasonal to seasonal (S2S) forecasting using the U.S. Naval Research Laboratory's (NRL) Earth System Prediction Capability (ESPC) is still in its infancy. The goal of Navy ESPC is to provide a high-resolution ensemble capability for the atmosphere and ocean out to 45 days (NRL 2021). However, only a few variables are currently available, and the accuracy of the forecasts is still uncertain. Considerable effort is needed to evaluate ESPC forecasts before it can be deemed a reliable forecasting tool.

C. PRIOR RESEARCH

Despite the appearance of a simple setup within the climate system, long-range forecasting (LRF) of the EAWM has proven to be somewhat difficult and continues to be a popular research topic of climate scientists. It is important to note that there are many studies regarding the synoptic, cold surge events associated with the EAWM. Most of these studies rely on daily data and address specific cold surge events. Prediction is limited in time, mostly out to the order of 1–2 weeks. Although our study will focus mainly on averaged monthly data, many important findings can be learned from the use of daily data and synoptic events. The 1978–1979 Winter Monsoon Experiment (Winter MONEX) was conducted to find several important factors of the East Asian Monsoon. This study connected the winds from the EAWM to convection near the island of Borneo, which helps prove the interconnectedness of the EAWM and other climate variables around the SCS region (Chang and Lau 1979). Park et al. (2011) used daily data to find a relationship

between the Arctic Oscillation (AO) and cold surges. They found that "cold surges during negative AO are stronger than those during positive AO in terms of both intensity and duration" (He et al. 2017). Ultimately, through an in-depth composite analysis, Park et al. (2011) was able to find a connection between the large-scale circulation patterns driven by the AO and cold surge strength.

Several studies also investigated how climate models, like the NCEP Climate Forecast System version 2 (CFSv2), predict synoptic cold surge events. Li et al. (2017) found that the CFSv2 model does a good job with "captur [ing] the frequency, intensity, and location of cold surges at a lead time of about two weeks" (Li et al. 2017). However, fewer cold surges were predicted past the 14 day lead time due to the complex nature of the atmosphere. Li et al. (2017) concluded that "possible causes of these biases and the impacts of initial atmospheric and oceanic conditions in the CFSv2 need to be further explored" (Li et al. 2017). Jiang et al. (2013) averaged the winter months of DJF to see how well the CFSv2 predicted the EAWM. Similar to the results from Li et al. (2017), CFSv2 captures most climatological features of the EAWM but still shows some biases. Figure 6 shows the plot of correlation coefficients between observed and hindcast values for the CFSv2 model from 1983–2010. CFSv2 shows high confidence in predicting El Nino/La Nina (ENLN) conditions out to a seven-month lead time, whereas there is low confidence in predicting the Arctic Oscillation (AO) index. The EAWM prediction falls in between ENLN and AO prediction with values greater than the 95% confidence level. However, it's important to see that the model does not do a perfect job in EAWM prediction. Many believe that turning to sophisticated, powerful computers will provide perfect forecasts, but this study proves that is not the case. Exploration into individual variables, geographic locations, and time scales are still required to assist LRF skill.

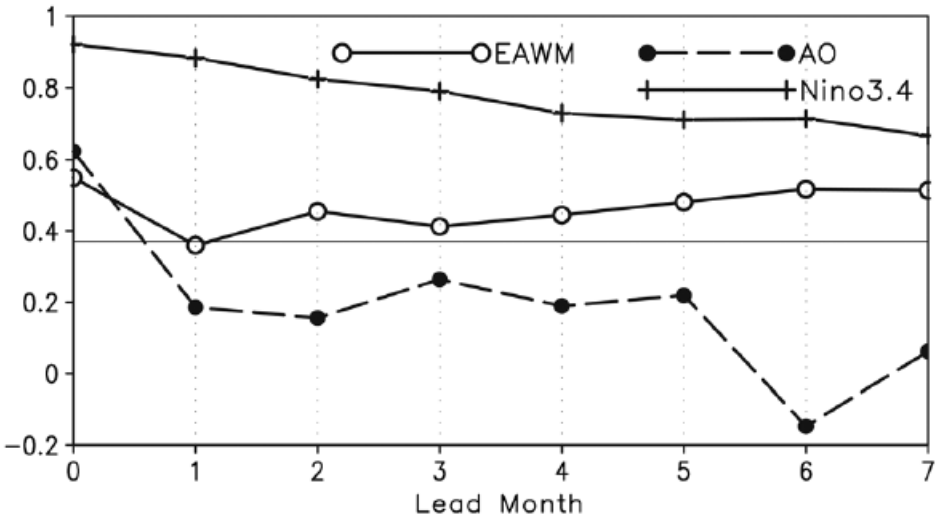

The solid line denotes the 95% confidence level.

Figure 6. Correlation coefficients between observed and hindcast values from CFSv2 from 1983–2020. Source: Jiang et al. (2013).

Over the past few decades, there has been significant progress in identifying the coupled air-ocean relationship centered around the equatorial regions. Research has shown that sea surface temperatures (SST) around the Equator can affect global climate patterns through a mechanism known as teleconnections (Bjerknes 1969). Bjerknes found that this equatorial teleconnection was associated with the Hadley circulation and the distant transportation of energy and momentum (Zhang et al. 1996). One of the most well-known teleconnections in climate science is the El Niño-Southern Oscillation (ENSO). ENSO has been linked to various phenomenon around the world, including various monsoon patterns. Prior research has investigated ENSO's impact on the EAWM (Zhang et al. 1996; Zhang et al. 1997; Wang et. al 2000). Zhang et al. (1996) found that southerly wind anomalies occurred along the East Asian coast during the 1986/87 and 1992/93 EN events. Through additional analysis, Zhang et al. (1996) suggests that the broader EAWM circulation can be traced to equatorial SST induced convection in the western tropical Pacific. Wang et al. (2000) expanded on the work from Zhang et al. (1996) and found a unique teleconnection between the central Pacific and EAWM. They determined "[t]he key system that bridges the warm (cold) events in the eastern Pacific and the weak (strong) East Asian winter

monsoons is an anomalous lower-tropospheric anticyclone (cyclone) located in the western North Pacific" (Wang et al. 2000).

While most previous work focuses on the tropical Pacific, a few studies have also included the Indian Ocean as a crucial piece of the EAWM (Annamalai et al. 2005; Kim et al. 2014). Using an atmospheric general circulation model (AGCM), Annamalai et al. (2005) found that more than "50% of the total precipitation anomalies over the tropical west Pacific-Maritime Continent is forced by remote Indian Ocean SST anomalies, offering an additional mechanism for the [EAWM-linked] Philippine Sea anticyclone apart from the Pacific SST" (Annamalai et al. 2005). Kim et al. (2014) found that the northern Indian Ocean plays a large role in the connection between the EAWM and ENLN/PDO.

In our study, we analyzed years of strong and weak EAWM winds in the SCS to assess the predictability of those variations at subseasonal to seasonal (S2S) lead times. We investigated the regional and global scale oceanic and atmospheric factors that trigger and contribute to the wind variations, such as variations in sea-surface temperature (SST) and sea-level pressure (SLP). We characterized the processes that generate both cool events (the S2S versions of synoptic cold surges) and warm events (the S2S versions of synoptic warm surges and the counterparts to synoptic cold surges). We also analyzed precursors to cool and warm events, and identified potential predictors of cool and warm events at S2S lead times. We have also investigated the influence of climate change on cool and warm events in the SCS (e.g., their intensity and frequency).

D. SCIENTIFIC GOALS AND RESEARCH QUESTIONS

Our work focuses on the SCS section of the EAWM to determine how these variables and indices work together or against each other to produce strong or weak northerly winds. Ultimately, we set out to achieve the following scientific goals:

1. Investigate regional and global oceanic and atmospheric factors that contribute to EAWM intensity within the SCS
2. Identify relationships between global scale climate variations and wind strength in the SCS

3. Identify the impacts of fluctuations in EAWM intensity around the SCS
4. Find possible teleconnections between SCS winds and global climate system
5. Develop and test methods to produce accurate S2S forecasts of the SCS winds
6. Determine how climate change will impact SCS wind strength in future decades

To achieve the scientific goals mentioned above, we wanted to answer the following research questions:

1. What are the large scale climate processes that drive variations in SCS meridional (v) wind intensity?
2. How do the fluctuations in SCS v wind intensity affect operationally relevant variables (waves, SLD, evaporation ducts, precip, etc)?
3. Are these variations in SCS v wind intensity predictable at S2S lead times (1 to 5 months)?
4. What indices are the best predictors for SCS v wind intensity? Do combinations of indices lead to better prediction?
5. How has climate change affected the SCS v winds and related atmospheric and oceanic variables?

II. DATA AND METHODS

A. DATA SETS AND VARIABLES

Reanalysis data sets were primarily used for this study. A reanalysis data set is a retrospective analysis of the climate system that uses modern analysis processes to evaluate previous states of the climate system (Kalnay et al. 1996; Murphree 2021a). Essentially, reanalysis data sets remove perceived spikes and discontinuities in climate variable time series that were due to different analysis techniques in the past. These data sets have been used extensively by climate scientists in previous studies to gain insight on the climate system throughout history.

1. NCEP/NCAR Reanalysis

The main climate data set used for this study is the NCEP/NCAR Reanalysis (R1) data set (Kalnay et al. 1996; Kistler et al. 2001). The R1 data set is the result of a retrospective analysis of global atmospheric variables that covers a date range of January 1948 to present. Data is collected from various sources, quality controlled, and assimilated with a data assimilation system (Kistler et al. 2001). The R1 data set has a spatial resolution of 2.5° (~210 km) and temporal resolution of six hours (00Z, 06Z, 12Z, 18Z) (Kalnay et al. 1996). The main variables we analyzed are winds (multiple levels), sea level pressure (SLP), sea surface temperature (SST), 1000 mb air temperature, 1000 mb specific humidity, outgoing longwave radiation (OLR), and 850 mb and 200 mb geopotential heights within the SCS region and globally. These variables were obtained from the NOAA/ESRL PSL website: (https://psl.noaa.gov/). As mentioned in Chapter I, we created several figures using the data access and product generation sites provided by the NOAA/ ESRL PSL, Boulder Colorado. These sites are accessible at: http://psl.noaa.gov/. In this research report, examples of these figures are indicated by the statement in the caption "PSL based figure."

2. ACAF Datasets

Multiple data sets from the ACAF website were utilized to provide an operational analysis for cool and warm events. Table 1 shows the maximum values possible for each data set. For our study, we focused on monthly averages at the maximum spatial resolution available.

Table 1. Data sets for ACAF variables. Adapted from FNMOC 2017.

Data Set	Variable	Region Available	Spatial Resolution	Temporal Resolution	Years Available for Analysis
Precipitation Estimation from Remotely Sensed Information using Artificial Neural Networks (PERSIANN)	Precipitation (inches or millimeters)	60°N-60°S Globally	0.25°	Daily	01 Jan 1983 to 31 Dec 2015
Climate Forecast System Reanalysis (CFSR) and CFSRv2	Total cloud cover (%)	Globally	0.3125° (~38 km)	Hourly	CFSR: 01 Jan 1979 to 31 Dec 2009 CFSRv2: 01 Jan 2010 to 31 Dec 2015
NOAA Wave Watch III (WWIII)	Significant wave height (SWH, ft)	Globally	0.5°	3 hourly data (03Z, 06Z, 09Z, 12Z, 15Z, 18Z, 21Z)	Jan 1980 to Dec 2007
CFSR Derived EM	Evaporation duct height (EDH, ft)	Western North Pacific (WNP): 10.15°S–50.11°N, 90°E-150°E	0.3125° (~38km)	Hourly	01 Jan 1979 to 31 Dec 2010
CFSR Oceanic Data	Sonic layer depth (SLD, ft)	Western North Pacific (WNP): 10.25°S–50.25°N, 89.75°E-150.25°E	0.25°	12 hours	01 Jan 1979 to 31 Dec 2010

3. Climate Indices

In our study we analyzed the relationships between multiple major climate indices and SCS v winds to help test potential predictors for cool and warm events.

a. NOAA Oceanic Niño Index (ONI)

As indicated in Chapter I, there is indication that ENLN plays a significant role in the strength of the EAWM. Since ENLN is such a widely studied climate phenomena, multiple indices have been created that capture the strength of ENLN events. For our study, we decided to focus on the ONI for our primary index. The ONI is a three month running mean of NOAA ERSSTv5 SST anomalies in the Niño 3.4 region (5°N-5°S, 120–170°W) (NOAA 2021b). The three month average of the ONI made it ideal to compare to a three month average (DJF) of the SCS v winds. ONI also incorporates a changing 30-year base period to account for a significant warming trend within the Niño 3.4 region. This made it ideal for our study since we analyzed 52 years of data from 1970–2021.

b. Arctic Oscillation (AO)

Prior research (Park et al. 2011; Chen et al. 2020) has identified AO as a potential predictor of the EAWM. We wanted to compare the SCS v winds with AO to determine the geographical extent of the AO on the winds. The AO is calculated with the daily 00Z 1000 mb height anomalies poleward of 20°N, which are then projected onto the loading pattern of the AO (NOAA 2021a). Monthly AO data was obtained from the National Weather Service (NWS) Climate Prediction Center (CPC)'s website at the following URL: https://www.cpc.ncep.noaa.gov/products/precip/CWlink/daily_ao_index/monthly.ao.index.b50.current.ascii.table.

c. North Atlantic Oscillation (NAO)

Chen et al. (2014) used NAO to find differences in the spatial differences in the EAWM. We wanted to determine how NAO correlates with our SCS v winds. The NAO is calculated by the north-south anomalies that range from Greenland to an area in the North Atlantic between 35°N and 40°N. More information on the climate variations

represented by the NAO can be found at https://www.cpc.ncep.noaa.gov/data/teledoc/nao.shtml.

d. Pacific North American (PNA) Index

The PNA is a teleconnection pattern within the northern hemisphere that captures the differences in heights throughout the Pacific and North American regions. These height changes work to cause differences in the climate system throughout the extratropics. More information on PNA can be found at https://www.cpc.ncep.noaa.gov/data/teledoc/pna.shtml

e. Pacific Warm Pool (PWP) Region

The PWP is an SST anomaly index calculated over the region of 60–170°E, 15°S-15°N (McKeon 2013). The index is calculated monthly and data is available from 1948-present. The values obtained for our study can be found at https://psl.noaa.gov/data/correlation/pacwarm.data

B. FOCUS REGION, FOCUS PERIOD, AND PREDICTAND SELECTION

1. Focus Region

As shown in Figure 1, we focused our study within the SCS. The coordinates within the SCS that we chose for this study are 8–18°N, 110–120°E. As indicated by the work of Jiang et al. (2013), there is reason to believe that various climate variables and indices influence the different geographic sections of the EAWM. We felt it was appropriate to analyze an area with a relatively small latitude/longitudinal extent to focus on: (a) the primary area within the SCS that the U.S. Navy will most likely be conducting future operations; (b) the area in which the strongest average winter winds occurs, as depicted in Figure 2; and (c) a study that addresses a specific portion of the EAWM.

2. Focus Period

We focused our study on a 52-year period from 1970–2021. Although there is reanalysis data before 1970, there is a possibility for spurious pre-satellite data that could cause some inconsistencies in our results (Heidt 2009). Figure 7 shows the DJF 1000 mb

v winds within our focus region from 1970–2021. Note the various interannual changes of the wind speed. This 52-year period captures an abundance of high and low wind DJF periods that could be used in our study.

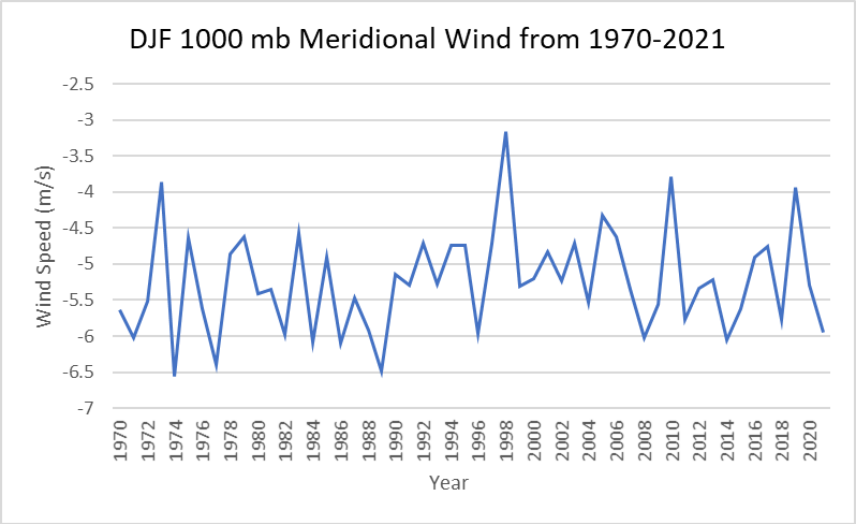

Figure 7. DJF 1000 mb v winds for our focus region (8-18°N, 110–120°E) from 1970–2021.

3. Predictand Selection

Previous studies (Chen et al. 2000; Wang and Chen 2014) have shown that the v wind strength is an effective index that provides valuable connections between the EAWM and climate system. After studying multiple time series (monthly, three-month averages, seasonal, etc.), we determined that the DJF period showed strong northerly wind values and considerable interannual variability. Within DJF, the month of January showed the strongest interannual variability (figure not shown). As such, we determined that the v wind values, as shown in Figure 7, are a legitimate index and could be used as a predictand for our study. With this v wind predictand for DJF and January, we developed and tested multiple LRF techniques.

C. ANALYSIS AND FORECASTING METHODS

1. Conditional Composites Analyses

After we determined that the time series for DJF v winds in the SCS from 1970–2021 was a sufficient predictand, we broke up the time series into above normal (AN), below normal (BN), and near normal (NN) terciles. In doing so, we identified the 17 AN events, 17 BN events, and 18 BN events. For our research, for the DJF v wind time series, we called the AN events our DJF warm events and BN events our DJF cool events. The result of breaking Figure 7 into terciles can be seen in Figure 8.

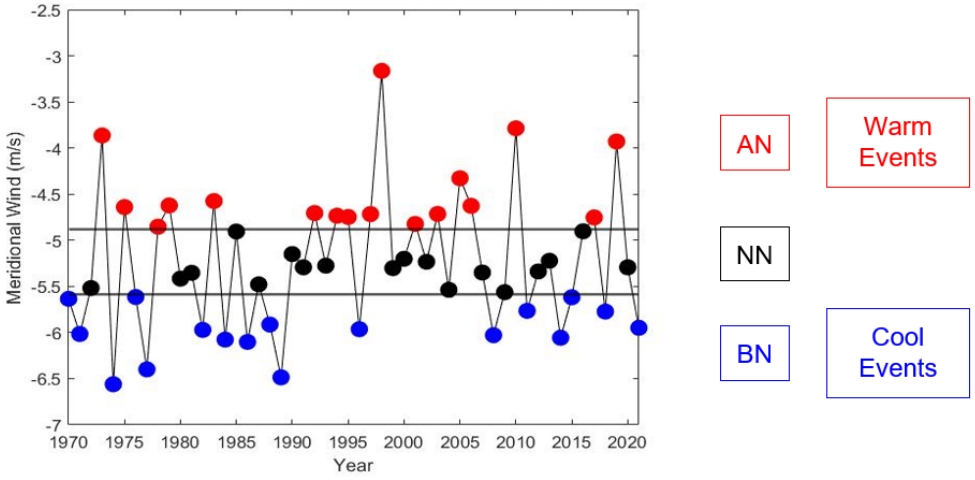

The black horizontal lines denote the threshold for the upper (warm events) and lower (cool events) terciles. The red circles denote years that correspond to warm events and the blue circles denote years that correspond to cool events.

Figure 8. Terciles for the 1000 mb v winds in the SCS for DJF 1970–2021.

With the DJF cool and warm events identified, we conducted conditional composite analyses of the cool and warm events to identify key features within the global and regional climate system. A conditional composite compares the years of cool and warm events with the LTM values to help highlight key features that could be useful in long-range forecasting. This technique is quite common among climate research and has provided useful results in prior research (Stone 2010; Lemke 2010; McKeon 2013; Byrne 2018). The main variables we analyzed include: 1000 mb winds, sea level pressure (SLP), sea

surface temperature (SST), 1000 mb air temperature, 1000 mb specific humidity, outgoing longwave radiation (OLR), and 850 mb and 200 mb geopotential heights.

To provide a more operationally relevant analysis of cool and warm events, we conducted conditional composite analyses of variables that would be useful for naval planning and operations. We used the ACAF tool to create conditional composite for the January cool and warm events. Only January months were used for these plots due to the plotting restrictions within the ACAF tool. We primarily focused on significant wave height (SWH), sonic layer depth (SLD), evaporation duct height (EDH), precipitation, and cloud cover. Anomalies from the LTM for these variables can show the differences in operating in the SCS during cool and warm events. The extent of the anomalies could play a critical role in naval operations in the SCS.

2. Correlation Analyses

Correlations were used to find spatial and temporal relationships, and to identify teleconnections, dynamical processes, and potential predictors. For example, we used correlations between the SCS v winds and global SSTs to find connections that could lead to skillful long-range forecasts. Correlations have been widely used throughout climate work (Gong et al. 2001; He and Wang 2013; Byrne 2018; Jones 2021) as a technique to explore dynamical and physical relationships between variables. Despite having a simplistic equation, linear correlation computations can lead to powerful results. Essentially, linear correlation determines how two variables are related. The equation used to compute the linear correlations is listed below (McKeon 2013), where x and y in the equation correspond to the two variables being correlated.

$$Correlation\ coefficient = R = \frac{\sum(xy)}{\sqrt{\sum(x^2)\sum(y^2)}}$$

The correlation coefficient, R, also known as the Pearson correlation coefficient, falls on a scale of 1 to -1 (Wilks 2006). A correlation of 1 (-1) shows a perfect positive (negative) relationship between two variables. A positive correlation means that when one variable increases (decreases), the other variable tends to increase (decrease). A negative correlation means that when one variable increases (decreases), the other variable tends to

decrease (increase). More information regarding correlation coefficients can be found in Wilks (2006).

A visual representation of correlations can help determine potential predictors of a certain predictand, or in our case, the DJF v winds in the SCS. An example of a correlation plot using the PSL site from previous work can be seen in Figure 9.

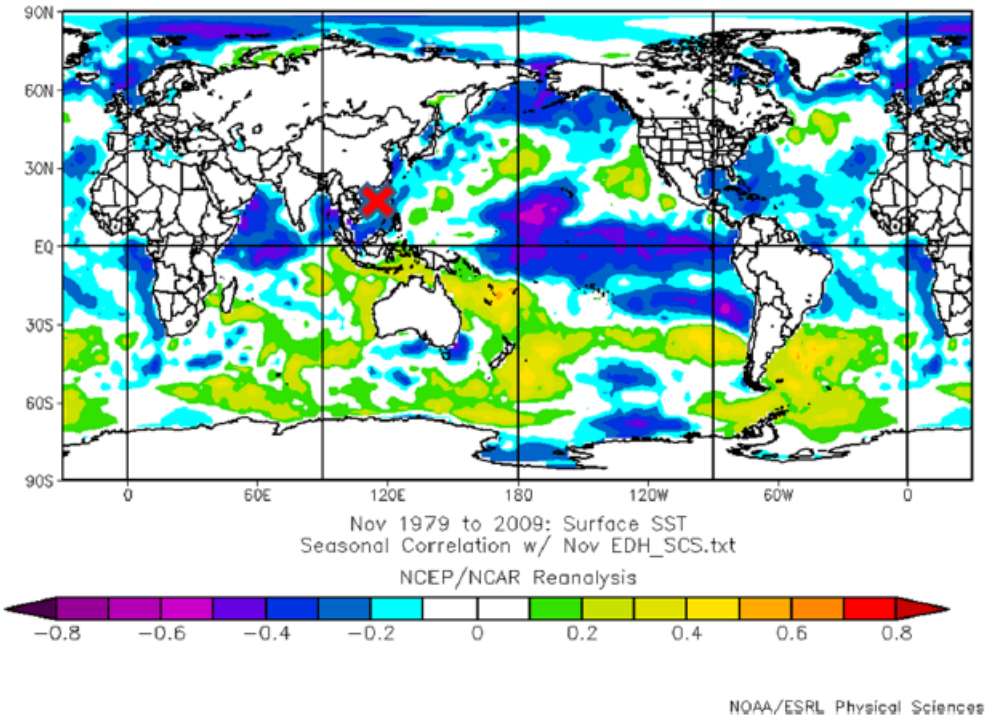

Figure 9. Example of a correlation plot between global SSTs and Nov EDH in the SCS. Source: McKeon (2013).

In Figure 9, the red "X" shows the Nov EDH in the SCS, or the predictand in this case. Areas of high positive (red) and high negative (purple) values could be potential predictor boxes of the Nov EDH in the SCS. Our work will use similar methods to find and test predictor boxes.

When conducting a statistical calculation, like linear correlation, it is important to identify the significance of your results. For our study, we will focus on the 99.5% confidence level. Based on 52 years of data, a correlation value of 0.370 and above is

statistically significant at the 99.5% confidence level (Livezey and Chen 1983; NOAA/ ESRL 2021). We chose 0.370 as the threshold for the predictors to be evaluated further using tercile matching or regression modeling.

3. Predictor Selection

We selected our predictors for this study based on several criteria: (1) The predictor must show a clear dynamical connection to the SCS v winds through our conditional composite and correlation analyses; and (2) A high correlation value of 0.370 or above that exceeds the 99.5% confidence level threshold for several months preceding the DJF period. Correlations were calculated for potential predictors from a zero-month lead to five-month lead using three-month averages (i.e., DJF, NDJ, OND, SON, ASO, JAS). The best predictors were narrowed down based on these correlation values. We calculated the lead time by determining the number of months between the middle of the predictor period to the middle of the valid period. For example, if the predictor period is JAS and the valid period is DJF, then the lead time is five months.

We also evaluated several climate indices that: (1) We saw evidence in our conditional and correlation analyses; or (2) Were investigated in prior work, but not necessarily used as a predictor at S2S leads.

4. Tercile Matching Method

Our first LRF method, known as tercile matching, has been used in previous studies (Heidt 2009; Lemke 2010; Byrne 2018) as a relatively simple yet effective way to generate forecasts for a predictand. Essentially, tercile matching forecasting uses the corresponding tercile of a set of predictor values to predict the tercile of the predictand value. For example, to predict the tercile of a predictand at a two-month lead, the set of known predictor values two months prior to the forecast period will be organized into terciles. Whichever tercile the predictor value falls under will be the forecast for the predictand two months in the future. With tercile matching, the sign of the correlation coefficient between the predictor and predictand determines the expected relationship between the predictor terciles and predictand terciles (Lemke 2010). For example, a positive correlation between the predictor and predictand means that the AN (BN) tercile for the predictor will forecast the AN (BN)

tercile for the predictand. On the other hand, a negative correlation between the predictor and the predictand that the AN (BN) tercile for the predictor will forecast the BN (AN) tercile for the predictand. If the tercile of the predictor matches the tercile of the predictand, the prediction is deemed correct.

5. Linear Regression Method

For our second LRF method, we used linear regression (LR) to identify the relationships between our predictors and predictand. LR is a widely accepted method within the climate community and can be seen in prior work (Lemke 2010; Stone 2010). Wilks (2006) explains LR and all the metrics in-depth. Still, at its simplest, "regression is most easily understood in the case of simple linear regression, which describes the linear relationship between two variables…" (Wilks 2006). When performing LR, the goal is to create an equation that can fit the data with the least error (Wilks 2006). This equation is then used to predict future predictand values. The equation is simply an equation of a line in the form:

$$y = b_0 + m_1 x_{1+\ldots}$$

where y is the predictand, b_0 is the y-intercept, m_1 is the coefficient of your first predictor, and x_1 is the first predictor value. There is an infinite number of additional predictors that can be used in one model. The next predictor would be $m_2 x_2$ and so on.

In our study, we used LR to create simple linear regression (SLR) models with one predictor and multiple linear regression (MLR) models with two or more predictors. Each SLR and MLR model generated a unique equation that could be used to forecast the value of the predictand. For example, one model consisted of the JAS, or 5-month lead, CTP SST box values from 1969–2020, and the actual DJF SCS v winds from 1970–2021. The LR process compared the SST values to the actual DJF SCS v winds to create an equation that can be used to predict future DJF SCS v winds. To evaluate each SLR and MLR, we analyzed two key statistics from the regression output, the R^2 values and p-values. R^2 quantifies the variance captured by our model's predictor(s). Like R, a high R^2 is ideal for a good model. A p-value is useful in comparing with the significance level and helps

determine if you can reject the null hypothesis (Wilks 2006), or essentially to determine if your results are due to random chance. We used a significance level of 5% (or .05) to grade each p-value.

6. Hindcasting and Verification

The goal of our study was to skillfully predict the correct tercile (i.e., DJF cool, DJF warm, and DJF neutral events) of our SCS v winds predictand at long lead times. To determine how well our tercile matching and LR methods performed with these predictions, we generated hindcasts from 1970–2021 and verified these hindcasts using 2x2 contingency table metrics (Wilks 2006). Figure 10 is an example of the 2x2 contingency table used in evaluating the skill of our predictions. We focused on predicting the correct tercile of the DJF SCS v winds because predicting the actual SCS v winds at long lead times could lead to spurious results. However, if we're able to predict which tercile the SCS v winds will fall in at a few months lead time, operators could use these results to plan for v winds that are stronger (i.e., cool events), weaker (i.e., warm events), or close to (near normal) the LTM v winds.

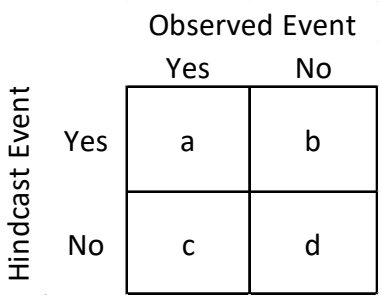

Figure 10. Example of 2x2 contingency table

As discussed in Chapter II Section C.1., we divided the values for our 52-year (1970-2021) DJF SCS v wind time series into terciles, which equates to 17 cool events, 17 warm events, and 18 near normal (neutral) events. For our tercile matching method hindcasts, we divided the values for our predictor's 52-year time series into terciles. After both the 52 predictor values and 52 SCS v wind values were organized into terciles, we

matched the predictor value for each year with the corresponding DJF SCS v wind value based on the correct sign from the correlation coefficient. We then scored each hindcast from 1970–2021.

As with our tercile matching method, the goal of LR was to skillfully predict the tercile of our SCS v wind predictand. For our SLR models, we divided the equation-generated DJF SCS v wind predictions from 1970–2021 into terciles (i.e., AN, BN, and NN). We then compared these predictions with the terciles of the actual SCS v winds to determine how well the regression performed. Like our tercile matching method, if the tercile of the predictor matched the tercile of the predictand, the prediction was deemed correct. For our MLR models, we performed cross validation using the "leave-one-out" (Wilks 2006) approach. This approach creates a more accurate model by "leaving out" the year we're predicting for out of the model. For example, to predict the 1970 DJF SCS v winds using JAS ONI and Borneo OLR values, we "left out" the 1969 JAS ONI, JAS Borneo OLR, and corresponding 1970 DJF SCS v wind values. We then ran the regression for years 1971–2021 to create a unique equation. Using this equation, we predicted the 1970 DJF SCS v winds. We repeated this process 52 times, one for each year from 1970–2021, for each combination of predictors at each lead time to generate cross validated DJF SCS v wind values. We then grouped all 52 DJF SCS v wind predictions by year, broke into their corresponding terciles, and performed the hindcasts by comparing the predicted tercile with the actual DJF SCS v wind tercile.

The main skill metrics we used were percent correct (PC), hit rate (HR), false alarm ratio (FAR), and Heidke skill score (HSS). The HSS helps to quantify how well the forecast performed against random chance, or the LTM in our case (Lemke 2010). The HSS provides a numerical result that ranges on a scale of -1 to 1. A perfect score is a 1 and the worst possible score is a -1. Anything less than zero means that your forecast doesn't perform any better than random chance, or the LTM. For the formulas and explanation of these metrics, see Wilks (2006).

To rank our predictions based on the 2x2 contingency table, we adopted statistical benchmarks used in prior research (Heidt 2009; Stone 2010; Lemke 2010). The thresholds are listed below:

1. PC values greater than 0.5 (or 50%).
2. HR equal to or greater than FAR.
3. HSS 0.300 or greater.

7. Multidecadal Analysis

We performed a multidecadal analysis because we noticed a trend within our DJF v wind time series, and we wanted to research how climate change has affected the DJF SCS v winds. In our study, we broke the DJF SCS v wind time series into two, 21-year periods. The first period was 1970–1990 and second period was 2001–2021. By using the ends of our time series, we can determine how the DJF SCS v winds have changed over our 52-year time series. We also created difference composite plots of multiple climate variables to determine the amount of change between the first period and most current period. Difference compositing is a common technique used in climate research (Kim et al. 2014; Jiang et al. 2013) that displays the visual differences between two data sets. To display the changes between the two periods, we utilized the difference composite plotting tool through the NOAA/ESRL PSL website. By understanding the multidecadal trend, we believe our results could improve LRF skill.

THIS PAGE INTENTIONALLY LEFT BLANK

III. RESULTS

As mentioned in Chapter II, we chose the 1000 mb v wind in the SCS as our predictor for this thesis. The technique of dividing the time series into terciles made it possible to analyze each tercile separately. We ultimately wanted to compare the cool event tercile with the warm event tercile. As mentioned in Chapter I, research on the EAWM tends to focus on the cool events while ignoring the warm events. However, our research shows that it is important to analyze both cool and warm events simultaneously to fully understand the problem. For this reason, we will be showing composite anomalies for both cool and warm events. Although many results will show a near mirror image to one another, there are subtle spatial differences within each variable that can be used to glean useful results.

The 1000 mb v wind time series broken up into terciles can be seen in Figure 8. It is important to note that we are working with negative values of the v wind for the entire time series. Negative values correspond to northerly winds. The least (most) negative values are the weaker (strongest) winds from the north. The full list of DJF cool and warm events can be found in Table 2. Composite analyses were not conducted for the near normal events, but were factored in the hindcasting portion of this thesis discussed later in this chapter.

Table 2. DJF cool and warm events from 1970–2021.

DJF			
Cool		Warm	
1970	1989	1973	1998
1971	1996	1975	2001
1974	2008	1978	2003
1976	2011	1979	2005
1977	2014	1983	2006
1982	2015	1992	2010
1984	2018	1994	2017
1986	2021	1995	2019
1988		1997	

A. CONDITIONAL COMPOSITE ANALYSES

When conducting a conditional composite analysis, it can be useful to first look at the LTM of the variable of interest. The LTM will show the typical conditions, or climatology, that would be expected for that variable during the specified time range. Since the LTM is an average over a long period of time, typically a 30-year benchmark, that will show typical conditions for that area. However, conditions can deviate from climatology quite drastically and produce conditions far from what is expected. It is the amount of difference from the expected conditions that we're looking to quantify with this thesis.

Figure 11 is a zoomed-out version of Figure 3 that shows the LTM conditions for the DJF v winds. The purple/blue colors indicate winds from the north (negative values) and the orange/red colors indicate winds from the south (positive values). There is consistent northerly flow with maximum values on the order of 6–8 m/s in the vicinity of the SCS. The overall pattern of v winds is consistent with the pressure systems illustrated in Figure 4. For brevity, we will not be displaying the LTM figures for each variable we analyzed. Only the anomaly figures will be provided within Chapter III of this thesis.

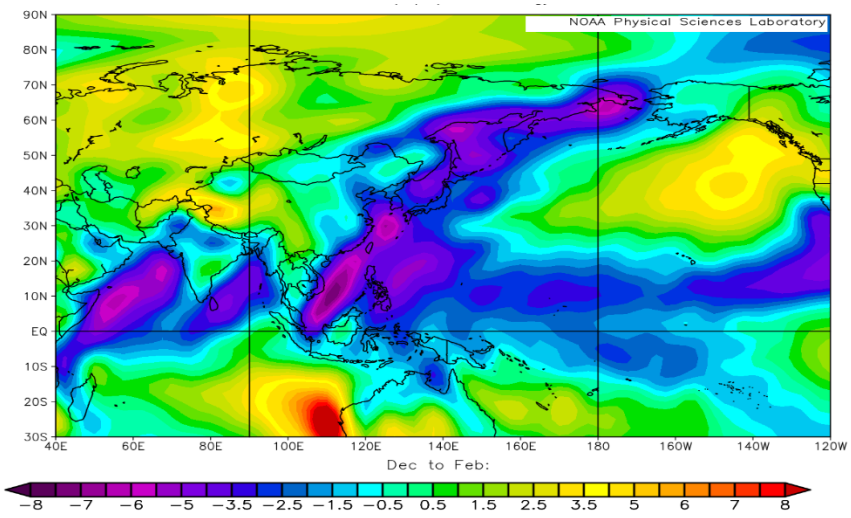

Figure 11. Long term mean (LTM) DJF v winds. PSL based figure.

1. 1000 mb Wind Anomalies

Figure 12 shows the 1000 mb wind anomalies for the entire Pacific basin. DJF cool (warm) events show negative (positive) wind anomalies in the SCS region. We found that the anomalies do not extend upwards to the Arctic region, indicating that the SH is not the only driver of the wind strength in the SCS. Prior EAWM research (Wang and Chen 2014) uses the strength of the SH as a predictor of wind strength. Our results indicate that this may not be the best predictor of the EAWM winds extending down into the SCS. We also found an interesting, Rossby wave-like pattern of v winds that extend from the Arctic down through the AL region to the U.S. west coast. The locations of these negative-positive-negative anomalies are nearly opposite for the cool and warm events. This further indicates the connection between winds in the SCS and other regions around the Pacific, specifically near the AL region.

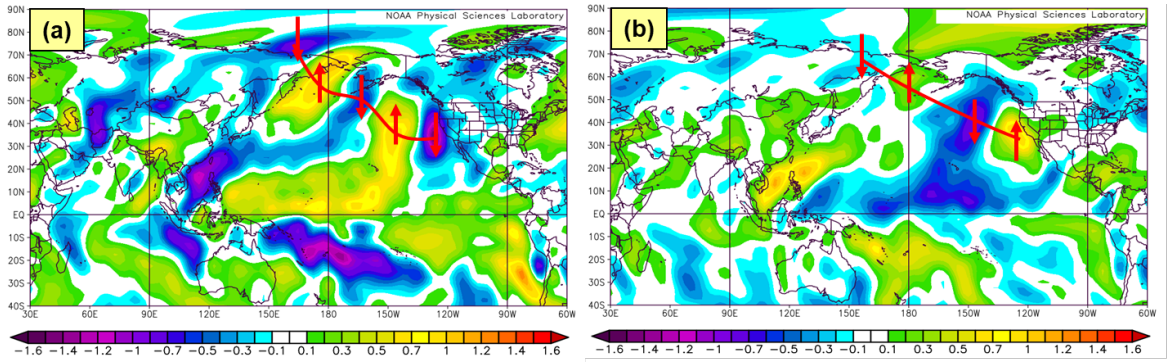

The negative values (purples, blues) represent northerly wind anomalies. The positive values (greens, yellows and reds) represent southerly wind anomalies. The red arrows in the figures show a pattern similar to a wave train in the extratropics.

Figure 12. The 1000 mb v wind (m/s) anomalies for: (a) DJF cool events (b) DJF warm events. PSL based figure.

2. SLP Anomalies

The next variable we analyzed was the SLP and its connection to the winds in the SCS. Figure 13 shows how the SLP anomalies (SLPAs) locations drive the flow through the SCS. During cool events, the pressure anomalies associated with the SH appear to be the greatest over western Asia, as indicated by the positive SLPAs. A stronger SH helps to

produce anomalous winds from the north along the Asian coast. Closer to the SCS, there is an area of positive SLPAs (purple circle) over the eastern portion of coastal China. However, the entire Asian mainland does not indicate positive SLPAs. There are areas of interior Asia that shows negative SLPAs. This result indicates that the coastal positive SLPA region is crucial for the occurrence of cool events. The other critical factor is the strength of the negative SLPAs (red circle) over the MC region. Without this pressure gradient, there would not be anomalous meridional flow. According to geostrophic reasoning, the overall anomalous flow is from the northeast during cool events, as indicated with the black arrow.

During warm events, areas of weaker positive and negative SLPAs indicate a weaker SH over interior Asia. This result matches our expectations as there is less flow directed toward the SCS from the north. Negative SLPAs (red circle) occur over the coastal China region while the positive SLPAs (purple circle) occur over the MC. The overall anomalous flow is from the southwest, opposite of the cool events.

We found strong anomalies for both cool and warm events around the AL. Positive (negative) SLPAs occur during cool (warm) events. These SLPAs are consistent with ENLN. This is one indication that cool and warm events connect to the tropical Pacific region. We will conduct a more in-depth analysis of the relationship to ENLN later in this chapter.

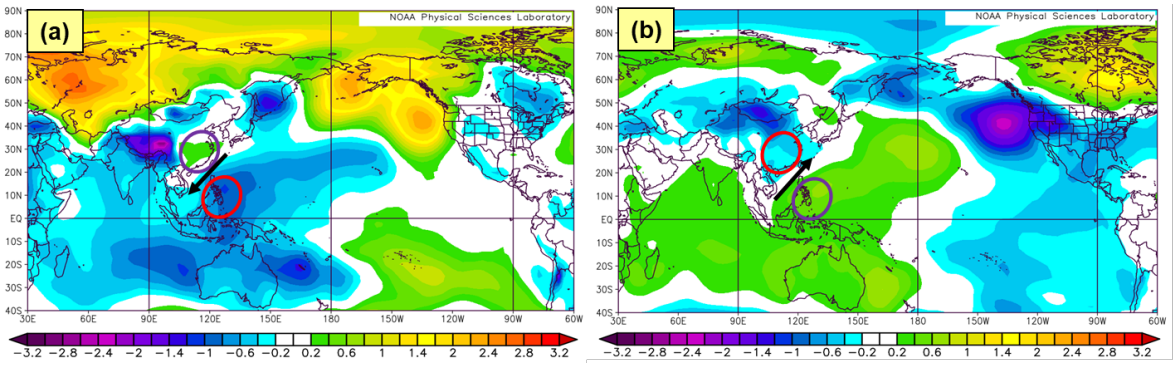

The purple circles denote areas of positive SLPAs. The red circles denote areas of negative SLPAs. The black arrow denotes the anomous wind direction.

Figure 13. SLP (mb) anomalies for (a) DJF cool events (b) DJF warm events. PSL based figure.

3. 850 mb Vector Wind Anomalies

Figure 14 shows how the 850 mb vector wind anomalies are associated with cool and warm events. There are distinct cyclonic (anticyclonic) wind anomalies above the MC and anticyclonic (cyclonic) wind anomalies near the Bering Sea during cool (warm) events. Warm events also shows a second area of anticyclonic wind anomalies in the central Pacific. Previous studies have performed 850 mb vector wind anomalies analyses during EN (Wang et al. 2000; He et al. 2013) and found similar locations to the cyclonic/ anticyclonic anomalies in our warm event analysis. These results further indicate a connection with the SCS v winds and the tropical Pacific region.

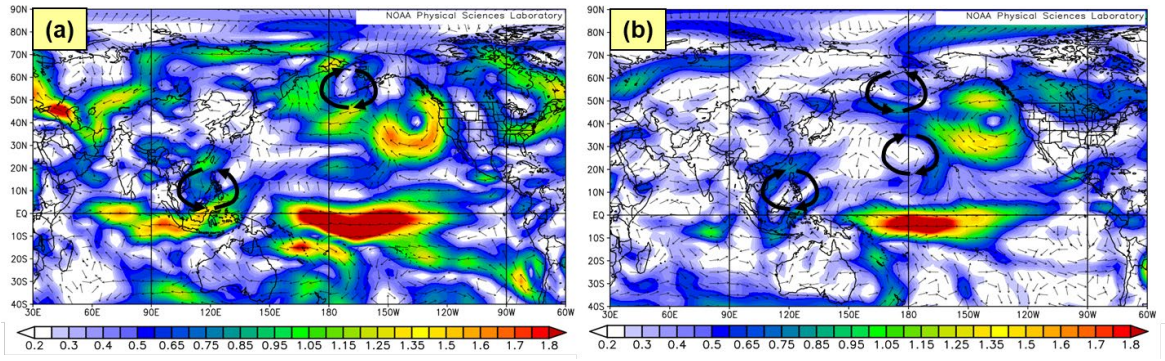

Figure 14. 850 mb vector winds (m/s) for (a) DJF cool events (b) DJF warm events. PSL based figure.

4. SST Anomalies

As indicated with our previous regional and global anomaly patterns, there is some evidence of a linkage between the SCS winds and the equatorial Pacific. Figure 15 shows how similar cool (warm) events are related to LN (EN). There is a large area of negative SST anomalies (SSTAs) extending from about 180° longitude to about 90°W, similar to LN conditions. Figure 16 shows the top 5 strongest cool/warm events vs. the top 5 strongest ENLN events. When comparing Figure 15 and Figure 16, cool (warm) events show LN (EN) tendencies. A more in depth statistical comparison between cool/warm events and ENLN will be described in Chapter III Section D.

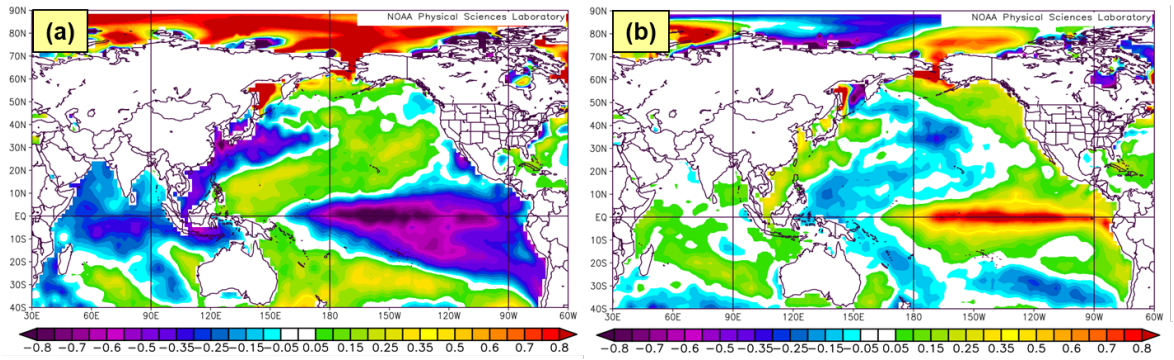

Figure 15. SST anomalies (K) for (a) DJF cool events (b) DJF warm events. PSL based figure.

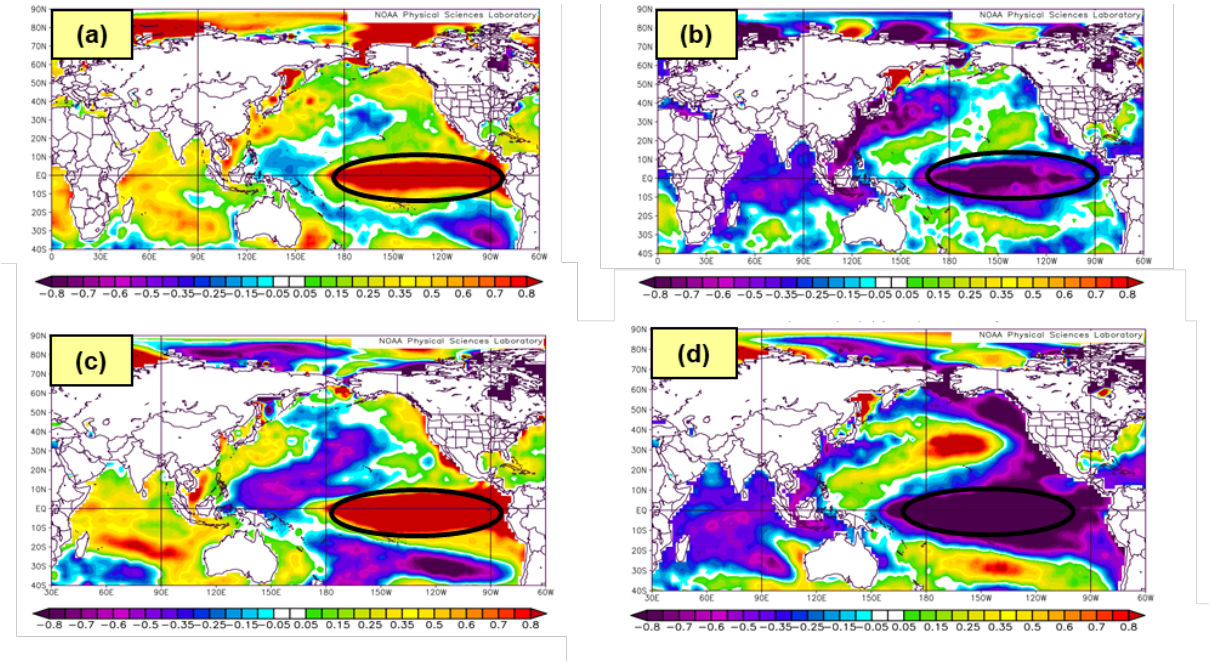

The black circles denote the area of the equatorial Pacific that are common between cool/ warm events and ENLN.

Figure 16. Visual comparison of cool/warm events to ENLN with: (a) Top 5 warm events (b) top 5 cool events (c) top 5 EN events (d) top 5 LN events. PSL based figure.

5. Air Temperature Anomalies

The air temperature anomalies for DJF cool and warm events are displayed in Figure 17. The DJF cool events show strong negative temperature anomalies extending from Siberia to the Asian coast through the SCS. This corresponds to the stronger

anomalous flow from the north during cool events. The negative temperature anomalies seem to follow the coastline down to about the Equator. The MC experiences positive temperature anomalies during cool events. Our results reiterate the spatial scale of the winds associated with the EAWM. The DJF warm events show positive temperature anomalies that extend from the Equator and 100°E–110°E northward through the SCS along the Asian coastline. Negative temperature anomalies are present over the MC. It is also important to recognize the temperature anomalies over the tropical Pacific. The temperature anomalies for cool and warm events correspond to the SSTAs (Figure 15). This matches our dynamic reasoning that cooler (warmer) SSTAs leads to cooler (warmer) air temperature anomalies. Air/sea interactions influence the amount of heat transfer between the water and the atmosphere above it and our results support that process.

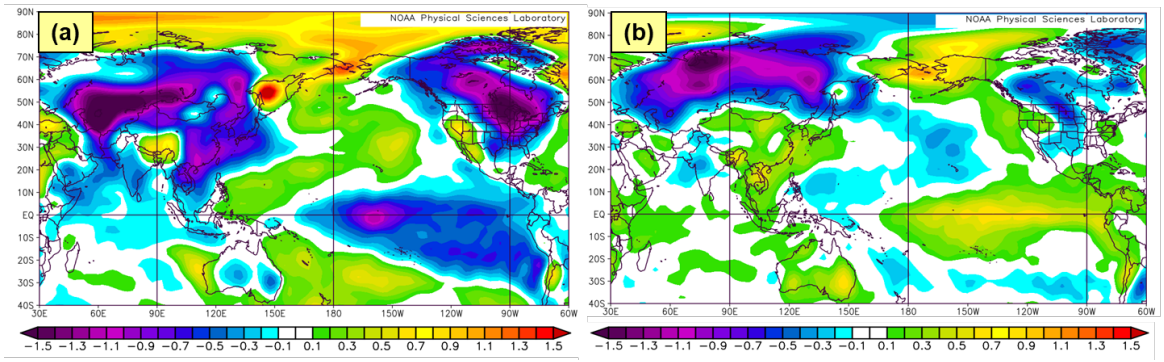

Figure 17. Air temperature anomalies (C) for (a) DJF cool events (b) DJF warm events. PSL based figure.

6. OLR Anomalies

We wanted to identify how cool and warm events are connected to clouds, moisture, and convection. To do this, we first conducted an analysis of OLR anomalies (OLRA). Figure 18 shows the differences between cool and warm events. For the cool events, negative OLRAs are present over the MC and positive OLRAs are present over the SCS and coastal China. The negative OLRAs around the MC and the Philippine Sea are consistent with the negative SLPAs (Figure 13) for cool events. Negative (positive) OLRAs indicate more (less) cloud cover and less (more) OLR reaching the top of the atmosphere.

Conversely, warm events show positive OLRAs over the MC and negative OLRAs over the SCS and coastal China. We also found a distinct "horseshoe" pattern of OLRAs for both cool and warm events, noted by the black line. This horseshoe extends from the midlatitudes off the coast of North America southwestward through the MC and southeastward toward South America.

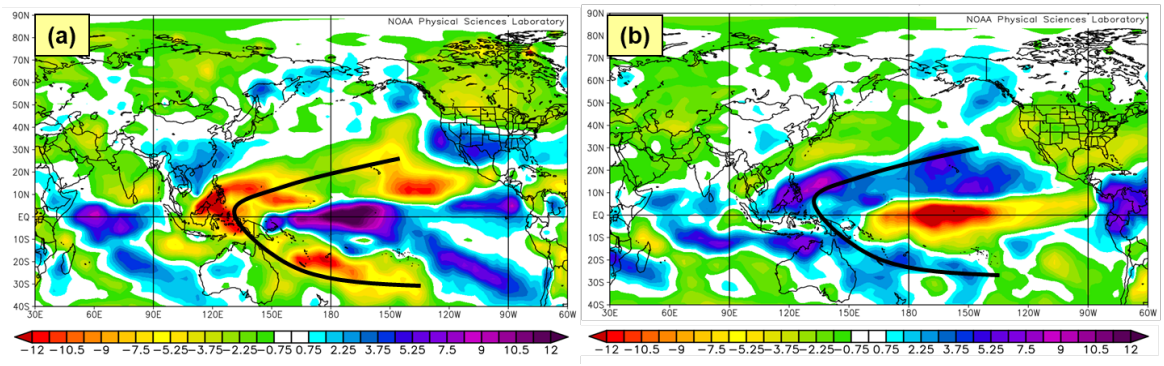

The black line denotes a commonly found "horseshoe pattern."

Figure 18. OLR anomalies (W/m2) for (a) DJF cool events (b) DJF warm events. PSL based figure.

7. Specific Humidity Anomalies

Figure 19 shows how the specific humidity values differ between cool and warm events. These patterns are consistent with the patterns that we observed in Figure 18. For cool events, negative specific humidity anomalies are located over the SCS. These negative anomalies are indicative of less cloud cover and moisture. For warm events, positive specific humidity anomalies are located over the SCS, indicating more cloud cover and moisture.

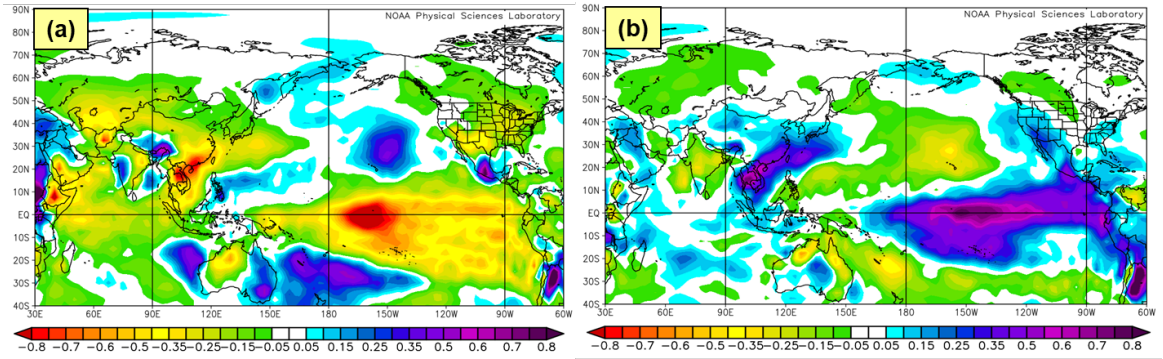

Figure 19. Specific humidity anomalies (g/kg) for (a) DJF cool events (b) DJF warm events. PSL based figure.

8. 200 mb Geopotential Height Anomalies

We wanted to conduct an analysis of the upper levels to determine if there is a connection between the upper and mid-latitudes and the tropical Pacific. Previous studies (Nitta 1987; Ford 2000) have discovered unique patterns that help drive processes thousands of miles away from the tropical Pacific. Figure 20 is an example of how warming in the western Tropical Pacific causes alternating areas of high and low pressures over the Pacific Ocean. These so-called teleconnections are critical in linking the earth's climate system. Figure 21 shows the eddy 200 mb geopotential height anomalies (ZA) for our study. We discovered unique anomalous Rossby wave trains in the northern hemisphere for both cool and warm events. Positive and negative anomalies are nearly opposite for the two cases. We also found a distinct wave train that emanates from the eastern tropical Pacific that extends upwards to the mid-latitudes for both warm and cool events. There is evidence that the processes that are causing v wind anomalies in the SCS are also causing anomalies elsewhere in the world, as shown by the extratropical anomalous Rossby wave train. There may be some feedback into the SCS region by the way of one of these wave trains, which we will investigate via a schematic later in this chapter.

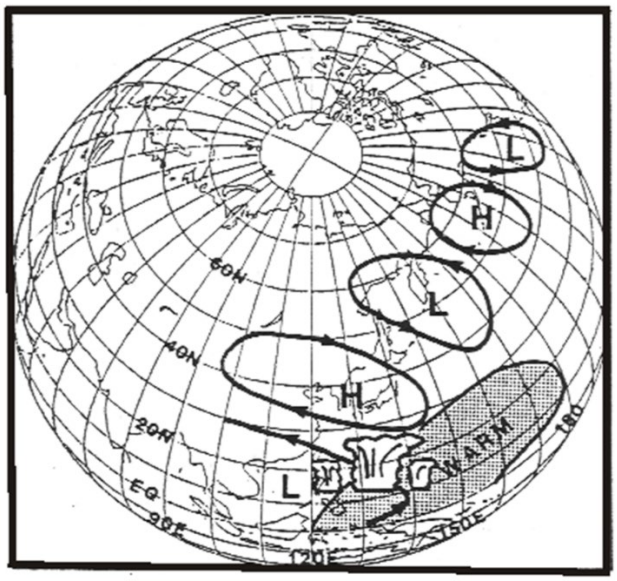

Figure 20. Upper tropospheric response to warming in the Tropical Pacific. Source: Nitta (1987).

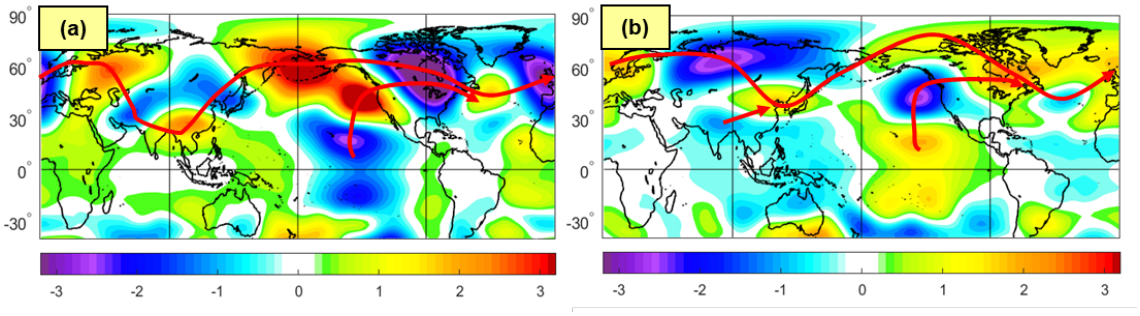

Figure 21. Eddy 200 mb geopotential height anomalies (gpm) for (a) DJF cool events (b) DJF warm events

B. ENVIRONMENTAL SETUP FOR COOL/WARM EVENTS

Before evaluated the S2S predictability of cool and warm events, we summarized our findings of the regional and global variables that are associated with cool and warm events. We created schematics (Figure 22 and Figure 23) that outline the climate variables associated with cool and warm events. It is important to note the spatial patterns with the various climate variables that we investigated. We investigated multiple variables from these spatial patterns that could serve as S2S predictors of the SCS v winds.

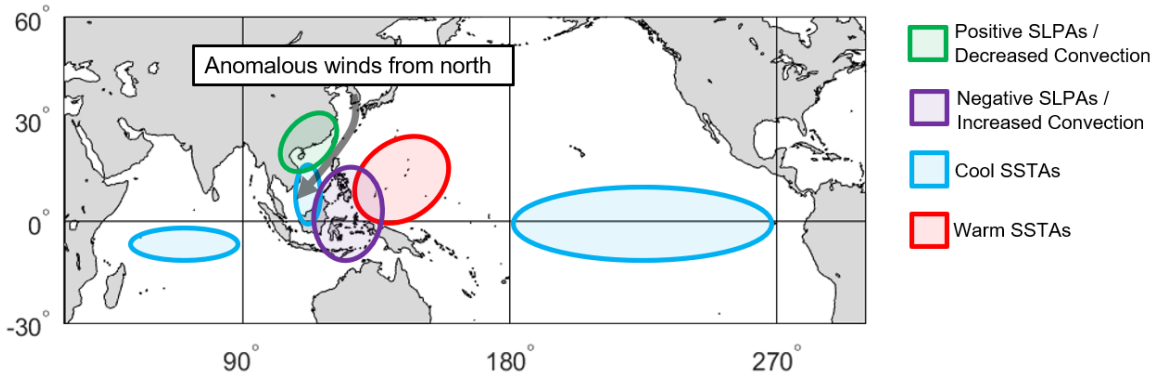

Figure 22. Schematic that summarizes cool event climate anomalies

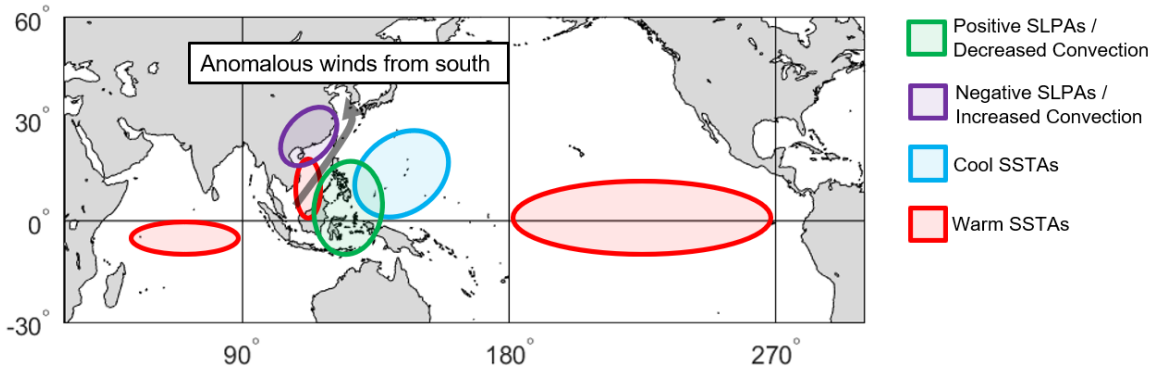

Figure 23. Schematic that summarizes warm event climate anomalies

Figure 24 and Figure 25 show a teleconnection pattern that connects the SSTAs in the tropical Pacific with the upper tropospheric anomalous Rossby wave trains we observed in our ZA200 analysis. During cool (warm) events, negative (positive) SSTAs suppress (enhance) convection in the eastern tropical Pacific, which decreases (increases) the height of the column of air above the region. These height changes perturb the overarching zonal flow in the mid and upper latitudes of the northern hemisphere, creating an anomalous extratropical Rossby wave train response. This is evidence of a similar response found in other climate research (Ford 2000; Kohlman et al. 2021). Although the SCS is located in the tropics, there is reason to believe that this Rossby wave train response affects the v winds in the SCS.

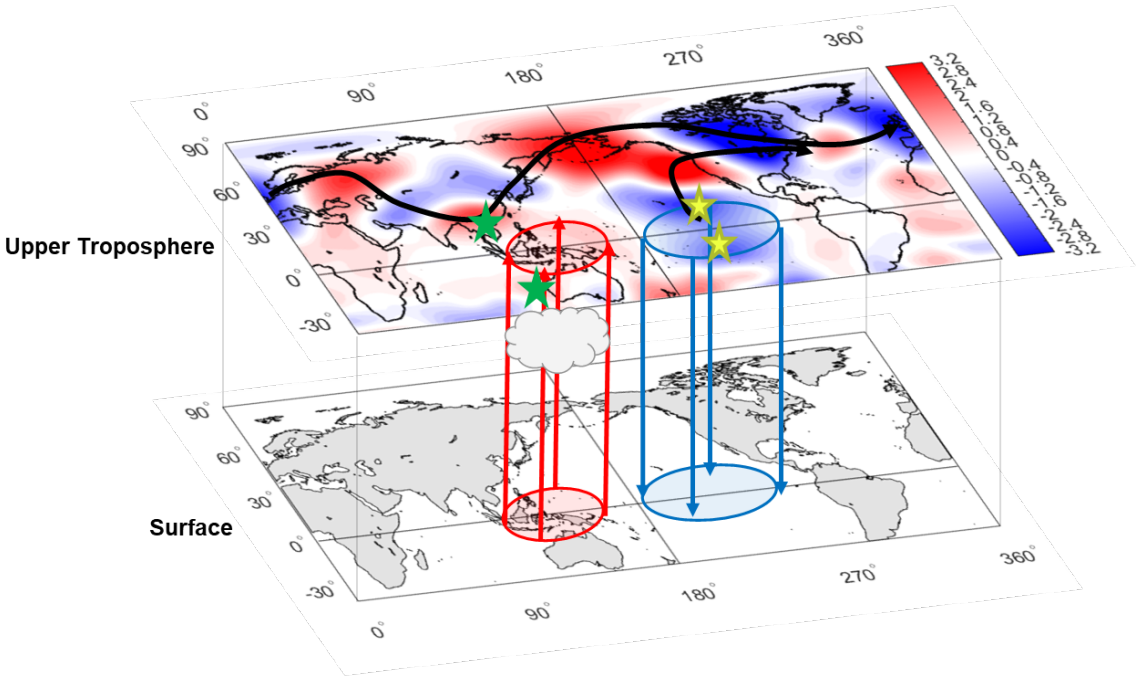

The bottom portion of the figure depicts the SSTAs for cool events. The red (blue) circles represent positive (negative) SSTAs. The upper portion of the figure depicts the eddy ZA200 heights and associated wave trains represented by the black arrows, one emanating from the eastern tropical Pacific and another from Southeast Asia. The yellow stars correspond to areas of anomalously low upper tropospheric heights and tropospheric cooling. The green stars correspond to areas of anomalously high upper tropospheric heights and tropospheric warming.

Figure 24. Schematic relating SST and upper tropospheric anomalies for cool events

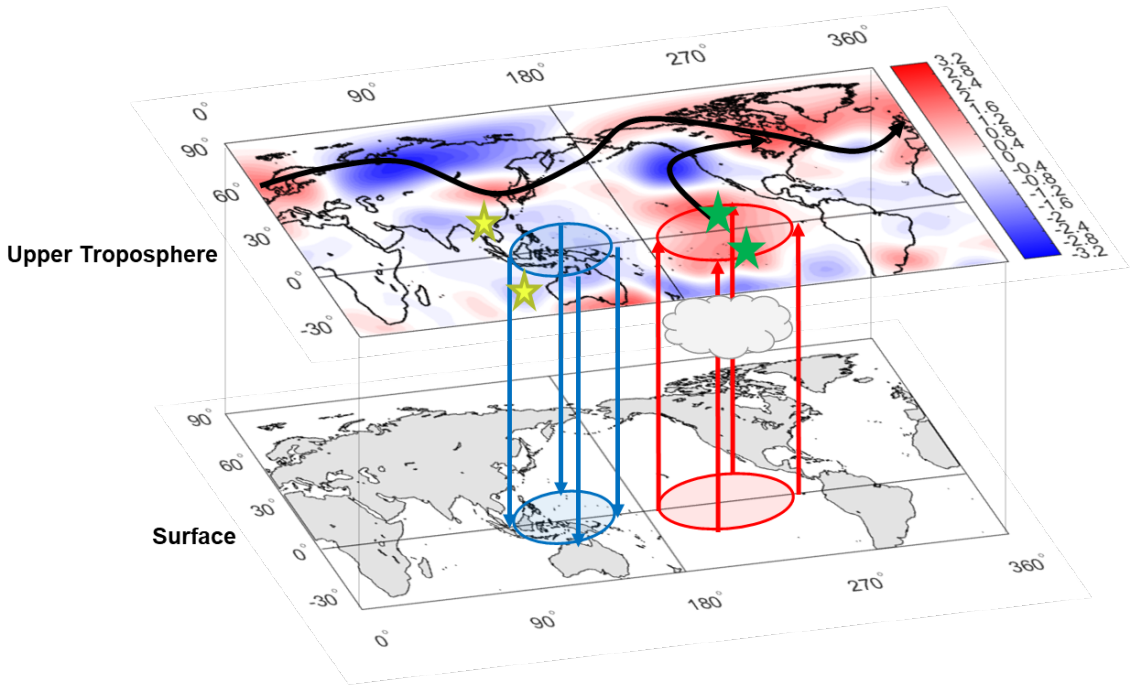

The bottom portion of the figure depicts the SSTAs for warm events. The red (blue) circles represent positive (negative) SSTAs. The upper portion of the figure depicts the eddy ZA200 heights and associated wave trains represented by the black arrows, one emanating from the eastern tropical Pacific and another from Southeast Asia. The yellow stars correspond to areas of anomalously low upper tropospheric heights and tropospheric cooling. The green stars correspond to areas of anomalously high upper tropospheric heights and tropospheric warming.

Figure 25. Schematic relating SST and upper tropospheric anomalies for warm events

C. OPERATIONAL VARIABLE COMPOSITE ANALYSIS

To provide more of a perspective on how cool and warm events affect naval operations and planning, we conducted a separate analysis to determine how operationally relevant variables change with the v wind strength. We utilized the ACAF plotting tool to obtain the next set of results. Due to plotting constraints within ACAF, we could only conduct single-month averages vice three-month (DJF) averages. We used the same methodology (Chapter II Section C.1) to identify the January cool and warm events via the January v wind time series. The January SCS v wind time series broken into AN, BN, and NN terciles can be seen in Figure 26. Table 3 shows the January cool and warm event years from 1970–2021. Each data set is constrained by a range of years available for plotting.

Table 1 shows the range of years available for ACAF plots, and we used the maximum amount of years possible in our results.

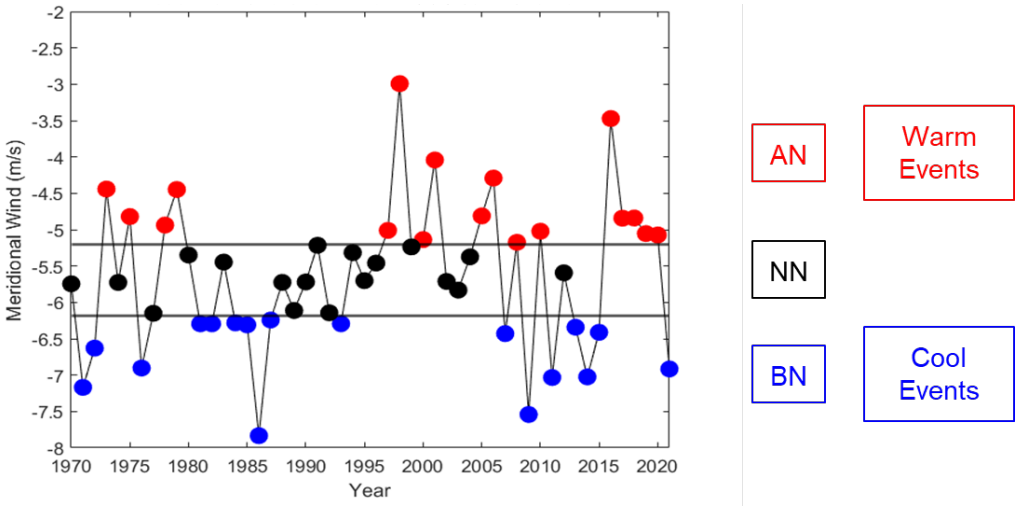

Figure 26. Terciles for the 1000 mb v winds in the SCS for Jan 1970–2021

Table 3. Jan warm and cool events from 1970–2021

Jan			
Cool		Warm	
1971	1987	1973	2006
1972	1993	1975	2008
1976	2007	1978	2010
1977	2009	1979	2016
1981	2011	1997	2017
1982	2013	1998	2018
1984	2014	2000	2019
1985	2015	2001	2020
1986		2005	

1. Significant Wave Height Anomalies

Figure 27 shows the significant wave height (SWH) anomalies for our January cases. During January cool events, the entire SCS region experiences positive SWH anomalies, which is to be expected with the stronger v winds from the north. We found that

the overall anomalies were quite low when compared to our expectations. This could be due to the limited fetch region north of the SCS. The average SWH anomalies across the region are about 1 ft. The highest anomaly of 1.5 ft occurs off the coast of Vietnam around 10°N 110°E. This region of highest seas corresponds to the far side of the fetch area that is experiencing the stronger northerly winds.

When the winds are anonymously weak during warm events, the SCS experiences lower than normal SWHs. Similar to the cool events, the average deviation from normal is about 1 ft throughout the region. The lowest SWH is found in a similar area to the highest positive anomalies for the cool events.

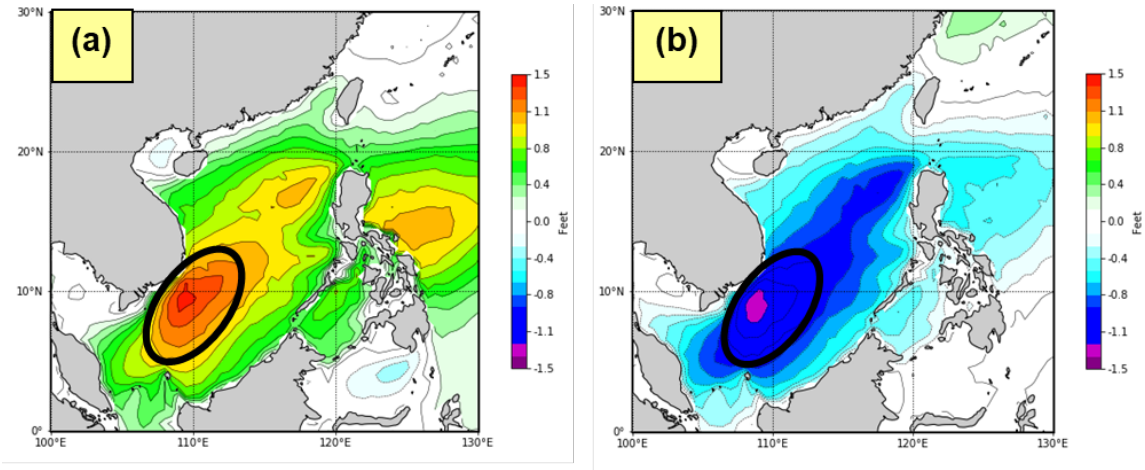

The black circles denote the areas of highest change from the LTM

Figure 27. Significant wave height (SWH) anomalies (ft) for (a) Jan cool events (b) Jan warm events

2. Sonic Layer Depth Anomalies

Previous studies have investigated SLD anomalies in moderately large areas like the western north Pacific (WNP) (Heidt 2009) and more confined areas like the SCS (Byrne 2018). We wanted to conduct a separate analysis using our unique methodology as discussed in Chapter II to determine the impact of cool and warm events on SLD. Figure 28 shows that the SLD is consistently deeper throughout the SCS, especially along about

12°N latitude. Anomalies during warm events exceed 50 ft over a few areas, as annotated by the red colors in the figure.

Warm events do not see similar orders of magnitude when compared to cool events. Throughout the SCS, there are small negative anomalies on the order of 0–15 ft. These results indicate that anti-submarine warfare (ASW) planners should understand that there could be a 50 ft difference in SLD between warm and cool events while operating in the SCS.

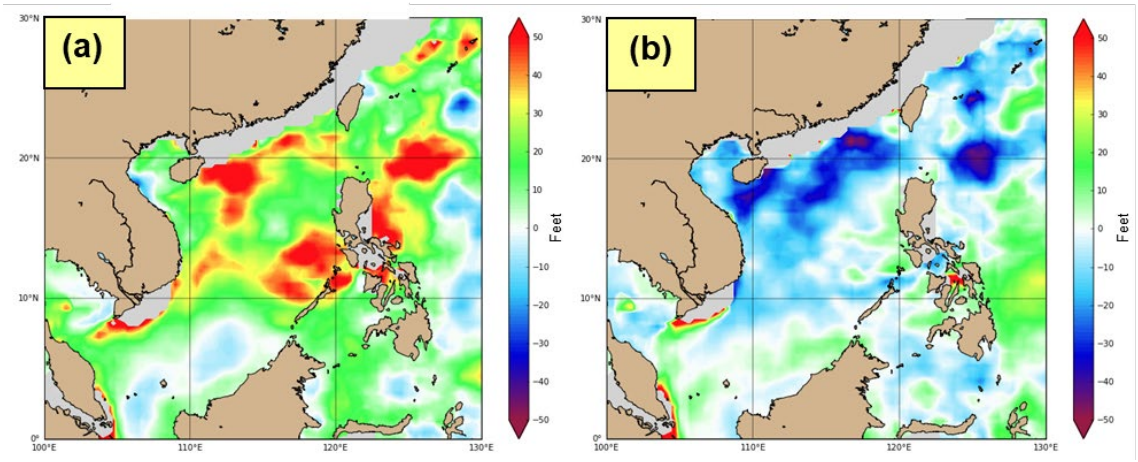

Figure 28. Sonic layer depth (SLD) anomalies (ft) for (a) Jan cool events (b) Jan warm events

3. Evaporation Duct Height Anomalies

The magnitude of evaporation duct height (EDH) anomalies can play a significant role in electromagnetic (EM) propagation (McKeon 2013). Figure 29 provides a visual representation of the differences in EDH for cool and warm events. Cool (warm) events are associated with higher (lower) EDH anomalies throughout the SCS. The greatest magnitudes occur off the Vietnam coast at the western boundary of the SCS. Users of the EM spectrum during cool (warm) events can expect improved (decreased) radar performances and ranges.

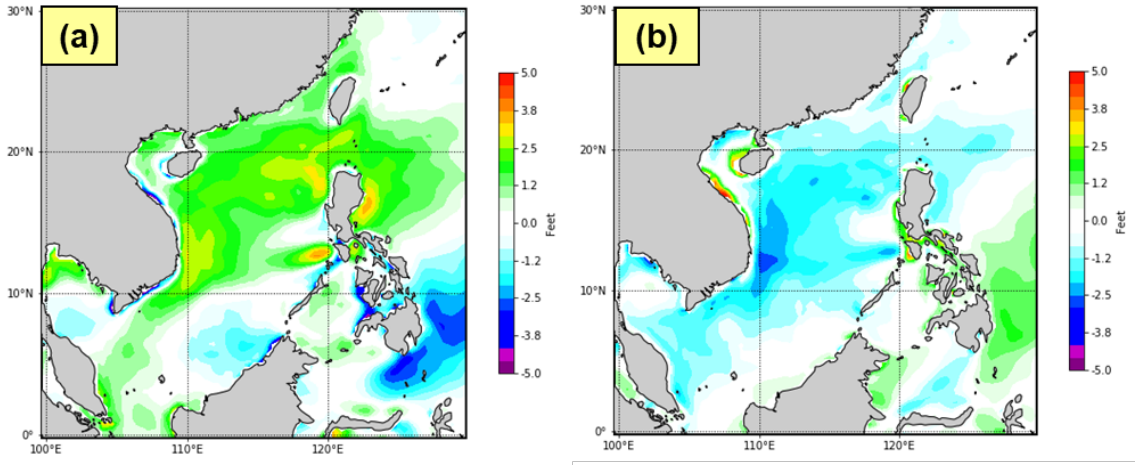

Figure 29. Evaporation duct height (EDH) anomalies (ft) for (a) Jan cool events (b) Jan warm events

4. Cloud Cover Anomalies

Differences in cloud cover can be operationally relevant when conducting intelligence, surveillance, and reconnaissance (ISR) missions or collection via satellites. Using the CFSRv2 dataset, there are noticeable differences between the cool and warm event cloud anomalies (Figure 30). The higher (lower) cloud cover percentages during cool (warm) events are consistent with our OLR analysis (Figure 18). A zoomed-out version of cool (warm) cloud percentage anomalies (Figure 31) shows negative (positive) values over the tropical Pacific that are consistent with LN (EN) conditions. We expected that would be the case considering our results up to this point in our research.

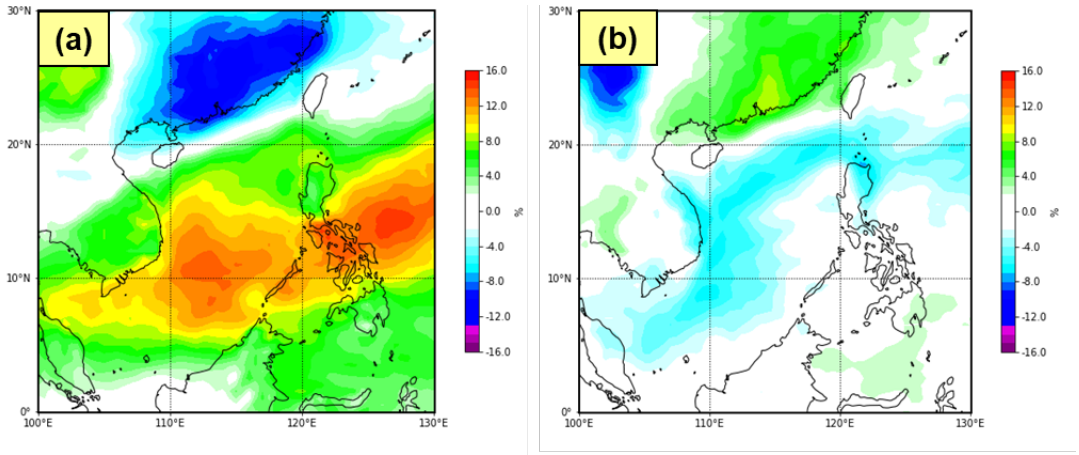

Figure 30. Cloud cover anomalies (%) over the SCS for (a) Jan cool events (b) Jan warm events

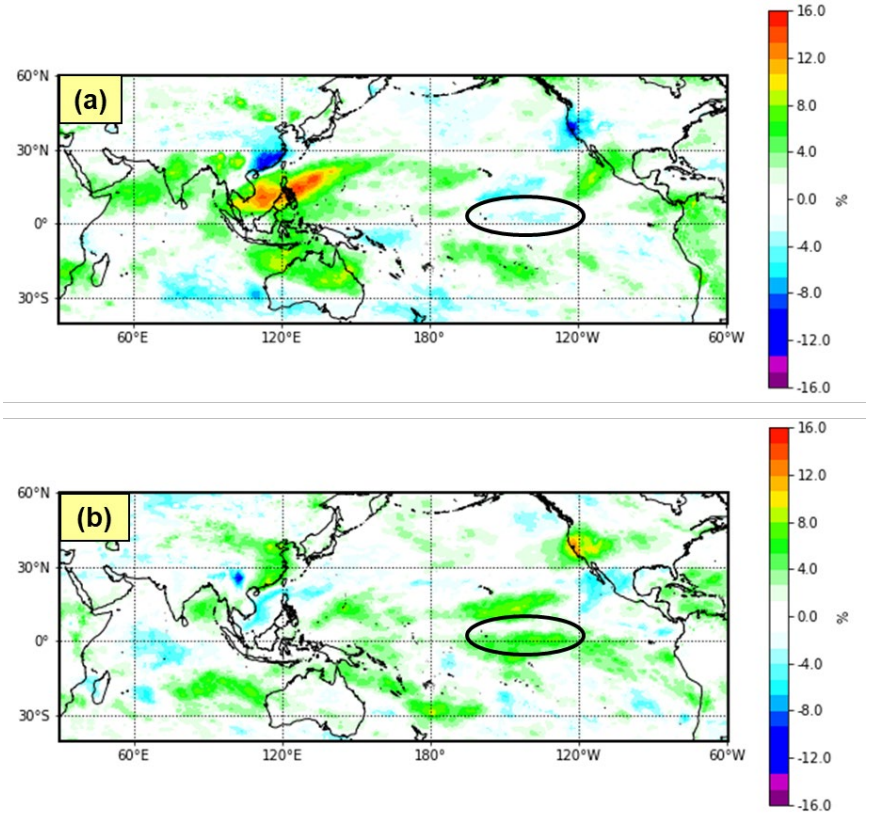

The black circles mark the areas of the equatorial Pacific where we saw ENLN tendencies with our SSTA results. The cloud cover anomalies match our expectations based on our SSTA results.

Figure 31. Indo-Pacific cloud cover anomalies (%) for (a) Jan cool events (b) Jan warm events

5. Precipitation Anomalies

After conducting a cloud analysis for cool and warm events, we wanted to discover how the cloud anomalies correspond to precipitation anomalies for the SCS and the greater Pacific regions. Figure 32 displays the cool and warm event precipitation anomalies over the SCS. For cool events, there are slightly positive (0.1 in.) precipitation anomalies over the southern portion of the SCS. Overall, we found that precipitation anomalies over the SCS were largely insignificant in an operational aspect. However, small anomalies have been known to cause significant impacts on the climate system at large. A more in-depth study of the precipitation anomalies could discover more effects on the climate system.

Figure 33 is a zoomed-out version of Figure 32. Negative (positive) precipitation anomalies occur over the equatorial Pacific for cool (warm) events.

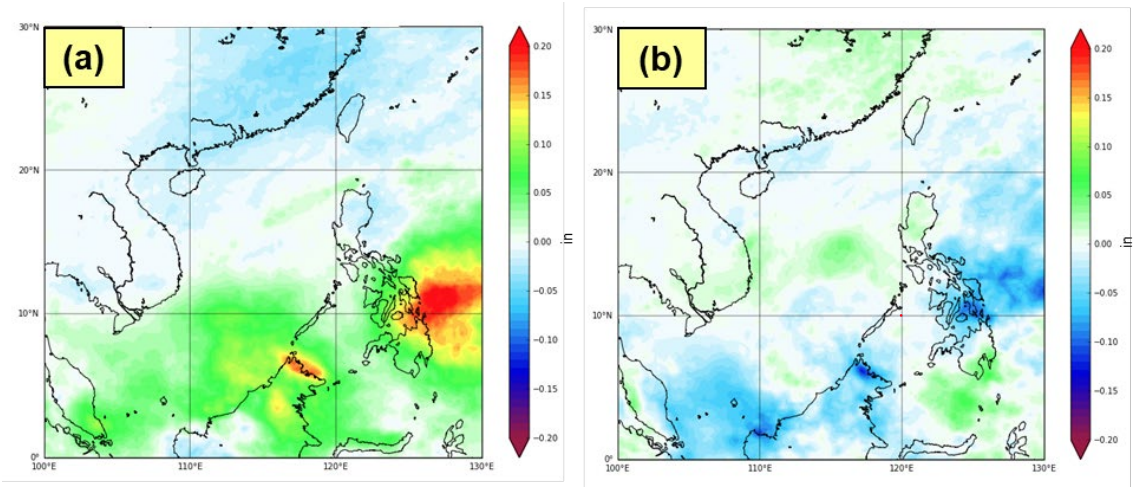

Figure 32. Precipitation anomalies (in.) over the SCS for (a) Jan cool events (b) Jan warm events

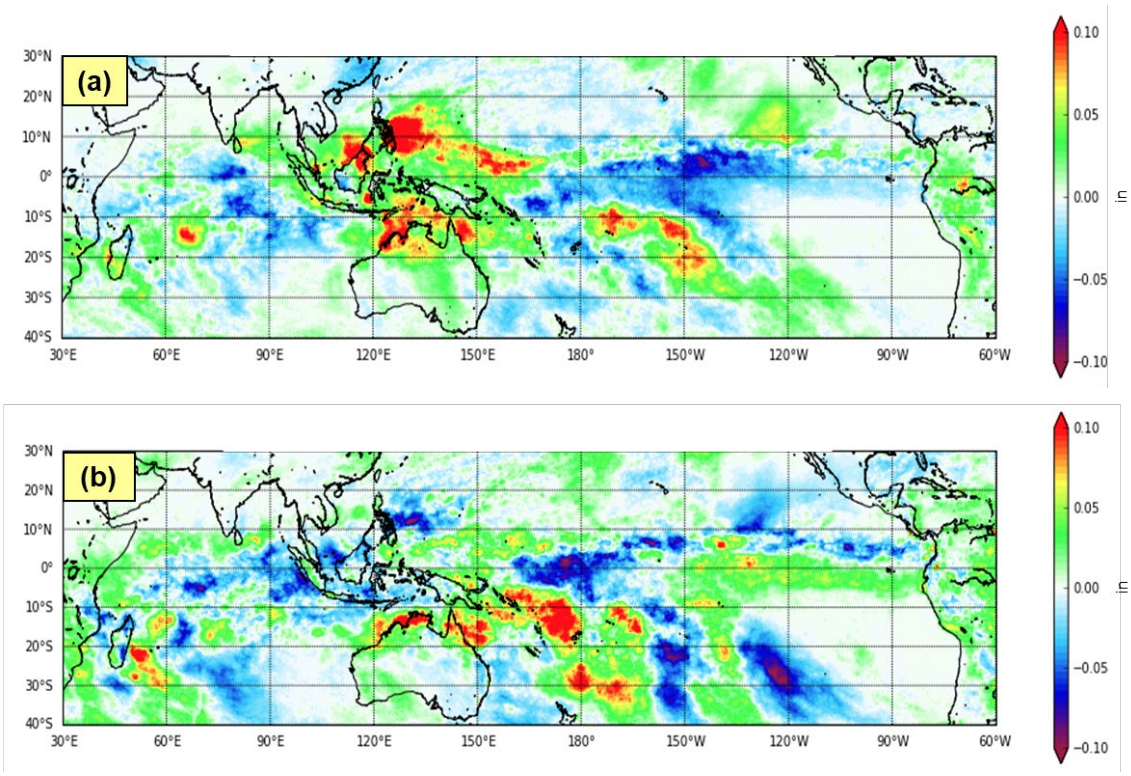

Figure 33. Indo-Pacific precipitation anomalies (in) for (a) Jan cool events (b) Jan warm events

D. RELATING COOL/WARM EVENTS TO ENLN

Our conditional composite analysis, along with prior research on the EAWM, has clearly shown a connection between the eastern tropical Pacific region and the intensity of the v winds around the SCS. To quantify this relationship, we conducted a statistical analysis to relate the different strengths of ENLN and the v winds. We created Table 4 by matching the 17 DJF cool events from 1970–2021 with the corresponding ONI ENLN category. We found that 11 of the 17 cool events occur during LN, or about 65%. Zero cool events occurred during strong ENs.

Table 4. Relationship between cool events and ENLN categories

ENLN Category	Ratio of # Cool event/ ENLN Combos to # Cool Events	Percentage
Strong La Niña (ONI ≤ -1)	7 / 17	41.2 %
Weak La Niña (-1< ONI ≤ -.5)	4 / 17	23.5 %
Neutral (-.5 < ONI < .5)	2 / 17	11.8 %
Weak El Niño (.5 ≤ ONI <1)	4 / 17	23.5 %
Strong El Niño (ONI ≥ 1)	0 / 17	0 %

We performed a similar analysis with warm events. Table 5 shows how warm events compare to ONI ENLN categories. We found that 10 of the 17 warm events occur during EN, or about 59%. Zero warm events occurred during strong LNs.

Table 5. Relationship between warm events and ENLN categories

ENLN Category	Ratio of # Warm event/ENLN Combos to # Warm Events	Percentage
Strong La Niña (ONI ≤ -1)	0 / 17	0 %
Weak La Niña (-1< ONI ≤ -.5)	4 / 17	23.5 %
Neutral (-.5 < ONI < .5)	3 / 17	17.6 %
Weak El Niño (.5 ≤ ONI <1)	4 / 17	23.5 %
Strong El Niño (ONI ≥1)	6 / 17	35.3 %

After conducting a simple comparison to see the quantitative relationship between DJF cool events and warm events, we completed an additional step to see how well ONI predicts cool and warm events out to 3 months. We found that ONI magnitudes of +/- 1 and greater do a reasonable job of predicting DJF cool and warm events. Tables 6–8 summarize our results. We performed a second prediction analysis with ONI using the tercile matching and linear regression methods explained in Chapter II, Sections C.4 and C.5. These results can be found in Chapter III, Sections F and G.

Table 6. DJF ONI prediction of DJF cool and warm events

DJF ONI Value	# of Occurrences 1970–2021	# DJF Cool events	Ratio Cool events/ ONI	# DJF Warm Events	Ratio Warm events/ONI
≤ -1.5	6	4	4/6 (67%)	0	0/6 (0%)
≤ -1	10	7	7/10 (70%)	0	0/10 (0%)
≤ - .5	21	11	11/21 (52%)	4	4/21 (19%)
≥.5	19	4	4/19 (21%)	10	10/19 (53%)
≥ 1	8	0	0/8 (0%)	6	6/8 (75%)
≥ 1.5	6	0	0/6 (0%)	5	5/6 (83%)

Table 7. NDJ ONI prediction of DJF cool and warm events

NDJ ONI Value	# of Occurrences 1970–2021	# DJF Cool events	Ratio Cool events/ ONI	# DJF Warm Events	Ratio Warm events/ONI
≤ -1.5	7	5	5/7 (71%)	0	0/7 (0%)
≤ -1	11	7	7/11 (64%)	0	0/11 (0%)
≤- .5	20	10	10/20 (50%)	4	4/20 (20%)
≥ .5	19	4	4/19 (21%)	10	10/19 (53%)
≥ 1	10	1	1/10 (10%)	7	7/10 (70%)
≥ 1.5	6	0	0/6 (0%)	5	5/6 (83%)

Table 8. OND ONI prediction of DJF cool and warm events

OND ONI Value	# of Occurrences 1970–2021	# DJF Cool events	Ratio Cool events/ ONI	# DJF Warm Events	Ratio Warm events/ONI
≤ -1.5	5	5	5/5 (100%)	0	0/5 (0%)
≤ -1	11	8	8/11 (73%)	0	0/11 (0%)
≤ - .5	20	10	10/20 (50%)	4	4/20 (20%)
≥ .5	19	4	4/19 (21%)	10	10/19 (53%)
≥ 1	10	1	1/10 (10%)	7	7/10 (70%)
≥ 1.5	4	0	0/4 (0%)	3	3/4 (75%)

E. CORRELATION ANALYSES

After we completed our conditional composite analyses, we performed correlation analyses between our predictand (1970-2021 DJF SCS v winds) and a series of potential predictors (climate variables and indices) from a zero-month lead time out to a five-month lead time. If the correlations between predictand and predictors remained highly significant throughout the zero-month lead to five-month lead time, we could potentially use the predictor in long-range forecasting.

We decided to conduct our first correlation analysis between our v wind predictand and global SSTs because: (a) the results from our conditional composite analysis show a dynamical connection between tropical SSTs and cool and warm events in the SCS; (b) global SSTs are known to drive variations in climate variables in other parts of the world; (c) changes in SSTs from month to month are slower than other climate variables; and (d) prior studies have found global SST regions to be a good LRF variable (Stone 2010; Lemke 2010; Vines 2017).

Figure 34 is a visual representation our correlation results from a zero to five-month lead time between our DJF SCS v wind predictand (dark blue box) and global SSTs. Figure 34 was created through the PSL website's correlation page: https://psl.noaa.gov/data/correlation/. We uploaded our custom SCS v wind time series to the PSL database to visually represent the correlation between SCS v wind and global SSTs. A full list of variables in which correlation plots can be created can be found on the correlation page listed above.

As discussed in Chapter II, we wanted to focus on correlation values of 0.370 (99.5% confidence level). We found four areas that maintained high correlation values throughout the five-month period by conducting a visual test. The following is a list of our SST predictor boxes: Central Tropical Pacific (CTP), Coral Sea (CS), and Western Indian Ocean (WIO). The coordinates and color of each predictor box in Figure 34 can be found in the caption under the figure. Although the WIO box (black box) does not represent the highest correlation values in the figure, prior research (Annamalai et al. 2005) indicated that the Indian Ocean plays a role in the dynamical processes of the EAWM. However, Annamalai et al. 2005 did not pursue LRF with an Indian Ocean SST predictor. For this reason, we wanted to find a unique SST predictor box in the Indian Ocean to test its LRF skill.

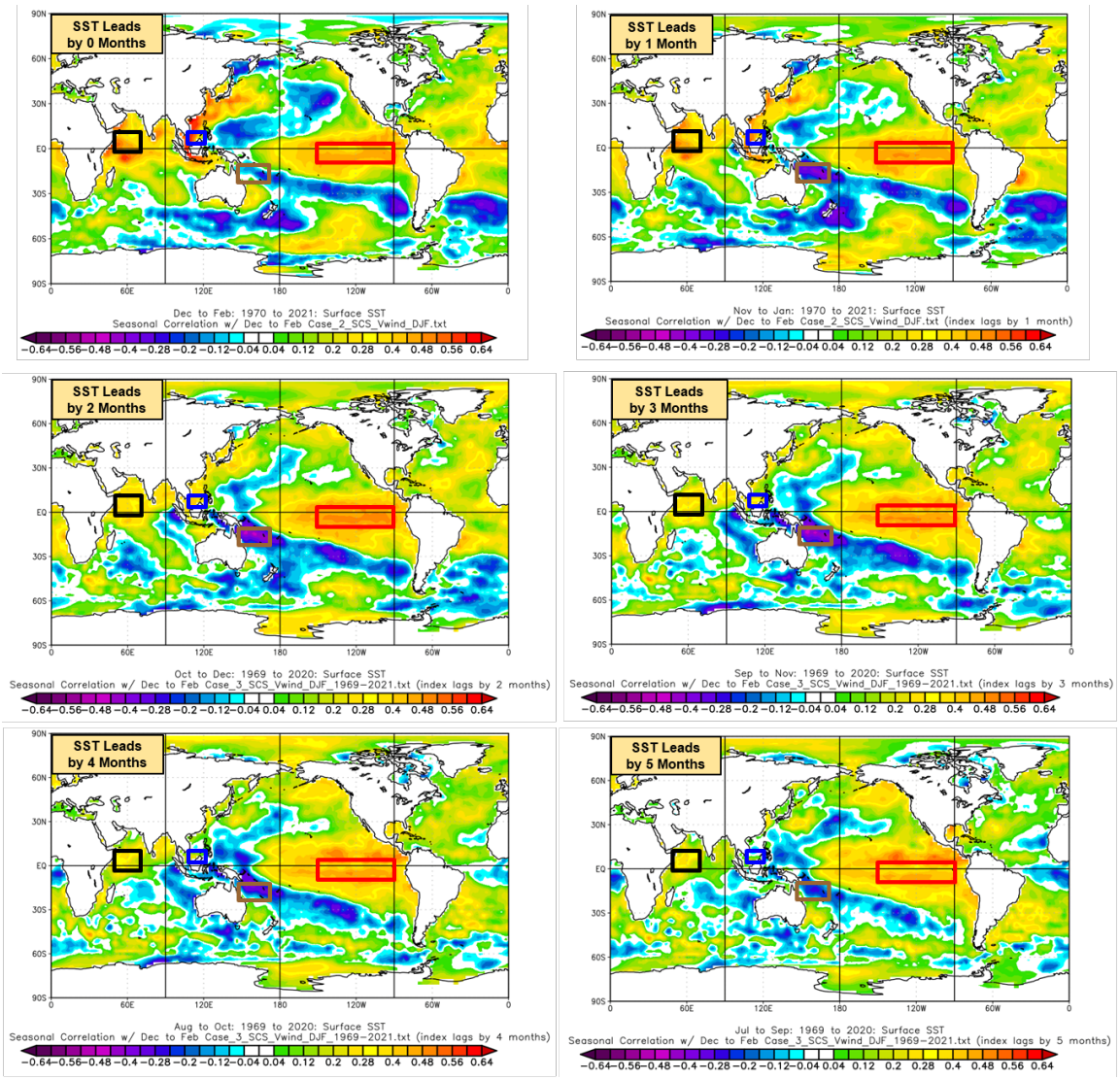

The dark blue box corresponds to our predictand SCS region (8-18°N, 110–120°E). The red box corresponds to the Central Tropical Pacific (CTP) region (5°N-10°S, 210–270°E-). The brown box corresponds to the Coral Sea (CS) region (12-21°S, 150–168°E). The black box corresponds to the Western Indian Ocean (WIO) region (0-10°N, 50–70°E). PSL based figure.

Figure 34. DJF SCS v wind predictand correlated with global SSTs (0-5 month lead)

After we determined three possible SST predictor boxes, we calculated the actual correlation coefficients of our DJF SCS v wind predictand and four SST boxes. High positive correlation values indicate when SSTs increase (decrease), the northerly v winds in the SCS decrease (increase). These results can be found in Table 9. Our results show

that the equatorial Pacific region is highly correlated with the SCS v winds. This matches with our results from Figure 34 and our previous analysis of the relationship warm and cool events with ENLN. We also found the lowest correlation values with the CS box and moderately strong correlation values with our WIO box.

Table 9. Correlation coefficients for the DJF SCS v winds and SST boxes

	DJF	NDJ	OND	SON	ASO	JAS
CTP SST Box	0.560	0.567	0.566	0.544	0.521	0.497
CS SST Box	-0.173	-0.448	-0.488	-0.491	-0.381	-0.282
WIO SST Box	0.470	0.416	0.327	0.327	0.286	0.233

	$\lvert R\rvert \geq 0.5$
	$0.4 \leq \lvert R\rvert < 0.5$
	$0.3 \leq \lvert R\rvert < 0.4$
	$0.2 \leq \lvert R\rvert < 0.3$
	$\lvert R\rvert < 0.2$

This table displays the correlation, R, values between predictors at 0–5 month lead times and DJF SCS v winds. We color coded the correlation values using the thresholds listed on the right.

After we completed our SST correlation analysis, we reviewed our conditional composite results and hypothesized that convection, especially around the MC region as indicated in Figure 18, could be a valuable predictor of the SCS v winds. Figure 35 shows the correlation values between the SCS v winds and global OLR. We identified two locations that maintained high correlations throughout the five-month period. The first location was in the vicinity of Borneo (black box) and second location was off the coast of Chile (red box). The strong correlation values off the coast of Chile indicate that there may be a distant teleconnection affecting the SCS v winds. Prior research (Schwing et al. 2002) has found teleconnections through the Hadley-Walker circulation (HWC) (Figure 36). While the HWC specifically looks at SLP, OLR can be related to SLP by indicating areas of clouds/low pressure (low OLR) and clear skies/high pressure (high OLR). Our OLR correlations indicate a similar structure to the HWC.

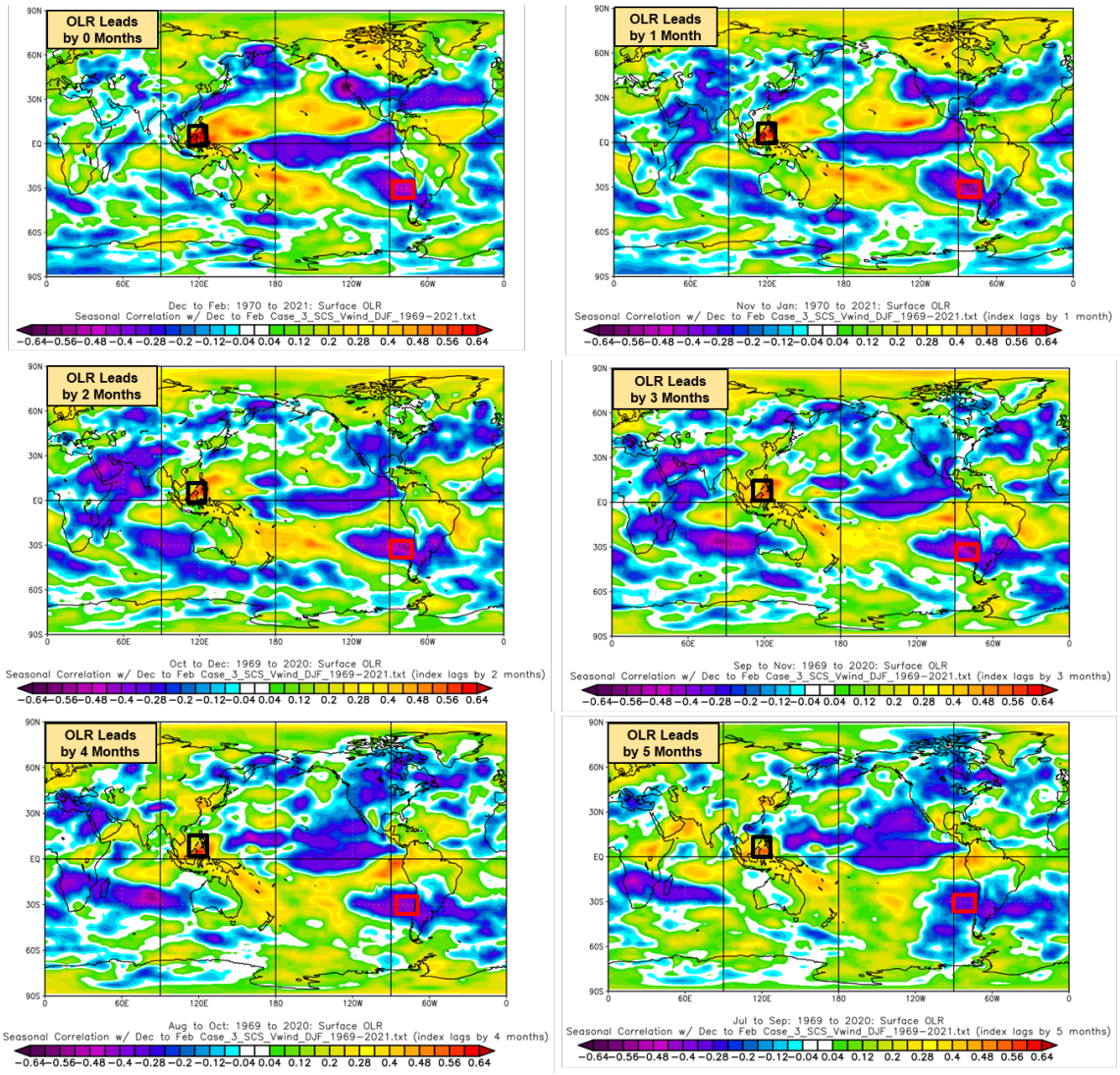

The red box corresponds to our Chile predictor (28-38°S, 85–75°W). The black box corresponds to our Borneo predictor (0-10°N, 115–130°E). We omitted our predictand SCS region (8-18°N, 110–120°E) box from this figure due to overlapping with our Borneo box. PSL based figure.

Figure 35. DJF SCS v wind predictand correlated with global OLR (0-5 month lead)

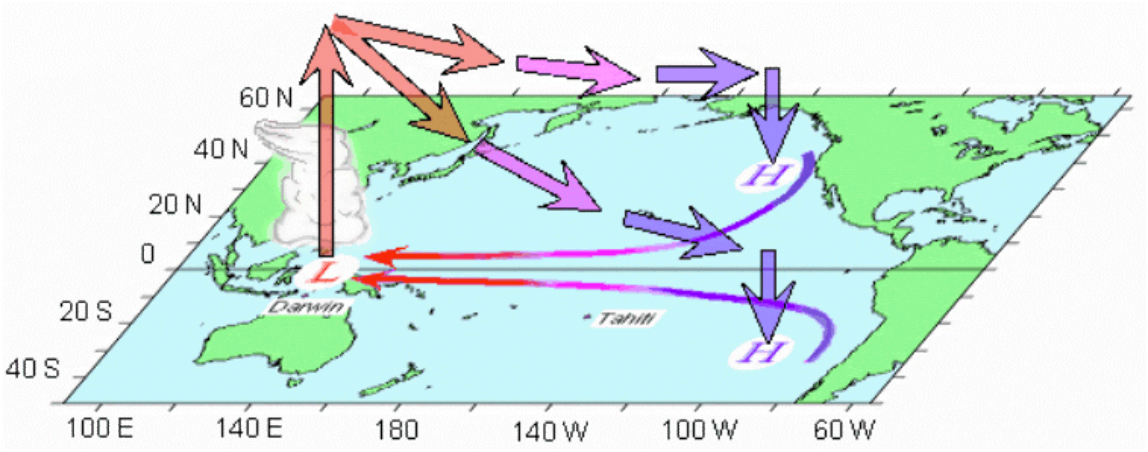

Figure 36. Hadley-Walker circulation for the Pacific Ocean region. Source: Schwing et al. (2002).

Similar to our SST correlation analysis, we calculated the correlation coefficients between the SCS v winds and our OLR predictor boxes. The results are summarized in Table 10.

Table 10. Correlation coefficients for the DJF SCS v winds and OLR boxes

	DJF	NDJ	OND	SON	ASO	JAS
Borneo OLR Box	0.710	0.650	0.571	0.570	0.564	0.543
Chile OLR Box	-0.508	-0.541	-0.504	-0.465	-0.394	-0.311

	|R| ≥ 0.5
	0.4 ≤ |R| < 0.5
	0.3 ≤ |R| < 0.4
	0.2 ≤ |R| < 0.3
	|R| < 0.2

This table displays the correlation, R, values between predictors at 0–5 month lead times and DJF SCS v winds. We color coded the correlation values using the thresholds listed on the right.

We also calculated the correlation coefficients between the SCS v winds and variable climate indices. Since ONI is calculated in three-month averages, we were able to compare ONI with our DJF SCS v wind time series. All other climate indices are calculated monthly, so we compared with our January SCS v wind time series. Those results are summarized in Table 11.

Table 11. Correlation coefficients for DJF/Jan SCS v winds and climate indices

	DJF	NDJ	OND	SON	ASO	JAS
ONI	0.579	0.567	0.561	0.549	0.534	0.523

	JAN	DEC	NOV	OCT	SEP	AUG
AO	-0.070	0.033	-0.015	-0.168	0.048	-0.152
NAO	0.156	0.046	0.085	0.196	0.087	0.101
PNA	0.033	0.227	0.116	0.195	0.052	0.181
PWP	0.340	0.231	0.126	0.066	-0.021	0.015

	|R| ≥ 0.5
	0.4 ≤ |R| < 0.5
	0.3 ≤ |R| < 0.4
	0.2 ≤ |R| < 0.3
	|R| < 0.2

This table displays the correlation, R, values between predictors at 0–5 month lead times and DJF SCS v winds. We color coded the correlation values using the thresholds listed on the right.

After we calculated the individual correlation coefficients for our list of predictors, we narrowed down the list to predictors that maintained a high correlation for the zero to five-month analysis. As stated in Chapter II Section C.2, we wanted to find predictors that maintained a correlation of 0.370 or above, which denotes a confidence level of 99.5%. Table 12 lists the four predictors we used in our hindcasting analysis. Although the five-month lead (JAS) correlation coefficient for the Chile OLR box falls under the 0.370 threshold we established, we felt that the correlations of all four preceding months were high enough to consider the Chile OLR box as a viable predictor. Although the CTP box and ONI are very similar geographically within the central Pacific, we wanted to identify any differences between the two predictors and determine which performs best with forecasting the SCS v winds.

Table 12. Final list of predictors used for hindcasting

Predictors	DJF	NDJ	OND	SON	ASO	JAS
CTP SST Box	0.560	0.567	0.566	0.544	0.521	0.497
Borneo OLR Box	0.710	0.650	0.571	0.570	0.564	0.543
Chile OLR Box	-0.508	-0.541	-0.504	-0.465	-0.394	-0.311
ONI	0.579	0.567	0.561	0.549	0.534	0.523

	|R| ≥ 0.5
	0.4 ≤ |R| < 0.5
	0.3 ≤ |R| < 0.4
	0.2 ≤ |R| < 0.3
	|R| < 0.2

This table displays the correlation, R, values between predictors at 0–5 month lead times and DJF SCS v winds. We color coded the correlation values using the thresholds listed on the right.

F. TERCILE MATCHING HINDCASTING

After we found our four best predictors, we used these predictors to create hindcasts from 1970–2021 using tercile matching. We next verified our hindcasts using the PC, HR, FAR, and HSS metrics described in Chapter II Section C.4. Table 13 summarizes the verification metrics produced by the hindcasts from a zero to five-month lead.

For the zero-month lead time (DJF) prediction of DJF cool events, our four predictors produced hindcasts that scored above our PC benchmark of 50%, had a HR greater than the FAR, and HSS greater than 0.300. Out of the four predictors, the hindcasts for the Borneo OLR box scored the highest PC score, highest HR, lowest FAR, and best HSS. For the zero-month lead time prediction of DJF warm events, the hindcasts using the CTP SST box saw a considerable drop in skill. We saw this through a FAR that exceeded the HR and an HSS less than 0.300. The hindcasts using the Borneo OLR box scored the highest across the board for PC, HR, FAR, and HSS. The second-best predictor of warm events was the ONI. The ONI hindcasts scored a 73.1% PC and 0.388 HSS. For the zero-month lead time prediction of DJF neutral events, the hindcasts for all four predictors scored the same across the board. It is important to note that prediction of neutral events is much more difficult than the cool and warm events. For this reason, we will only access the scores of the cool and warm events for the remaining lead times. Refer to Table 13 for remaining neutral event scores at one to five-month leads.

For the one-month lead time (NDJ) prediction of DJF cool events, the Borneo OLR box hindcasts again scored the highest out of the four predictors. The PC remained the same as the zero-month lead prediction (76.9%) and HSS of 0.476 did not change as well. For the one-month lead time (NDJ) prediction of DJF warm events, the skill of the Borneo OLR box hindcasts fell below both the ONI and Chile OLR box hindcasts. The NDJ ONI was the best at predicting DJF warm events with a PC of 73.1% and HSS of 0.388.

For the two-month lead time (OND) prediction of DJF cool events, hindcasts for the CTP SST box, Borneo OLR box, and ONI scored the highest for PC, HR, FAR, and HSS. The PC of 73.1% continued to be much higher than the 50% benchmark, even at a two-month lead. The HSS's of 0.388 remained 0.88 above our 0.300 benchmark. For the

two-month lead time (OND) prediction of warm events, the ONI and Chile OLR box hindcasts scored a 73.1% PC with HSS of 0.388. The CTP SST box hindcasts and Borneo OLR box hindcasts scored slightly lower for the warm event prediction with PC scores of 69.2% and HSS's of 0.301. Overall, the ONI predictor performs the best at a two-month lead.

For the three-month lead time (SON) prediction of DJF cool events, the results are very similar to the two-month lead time. The hindcasts for the CTP SST box, Borneo OLR box, and ONI maintained a 73.1% PC with 0.388 HSS's. For the three-month lead time (SON) prediction of DJF warm events, the hindcasts for the Borneo OLR box showed the highest PC at 76.9%. This is quite a high percentage despite a three-month lead time. Overall, the Borneo OLR box performed the best at predicting cool and warm events for the SON lead time.

At a four-month lead time (ASO), the hindcasts for the four predictors showed some decrease in PC when compared to SON. The hindcasts for the CTP SST box, Borneo OLR Box, and ONI produced scores of 69.2% PC with HSS's of 0.301. There was some decrease in the HSS from three to four-month leads, but the hindcasts for the four predictors maintained the 0.300 HSS benchmark. For the warm events, the Borneo SST box hindcasts and ONI hindcasts produced a PC of 73.1% and HSS of 0.388. At four-month lead times, the Borneo OLR and ONI are very similar predictors and either could be used in DJF SCS v wind prediction.

At a five-month lead time (JAS), the hindcast for the Borneo OLR box performed the best out of the four predictors at both DJF cool and warm event prediction. The metrics remained remarkably high at such a long lead time across the board for all four predictors, but the Borneo OLR box seemed to produce the best hindcasting results.

In summary, we performed hindcasts from 1970–2021 for our top four predictors using tercile matching and calculated verification metrics via 2x2 contingency tables. The hindcasts for all four predictors were compared to one another using our criteria for successful predictors (PC 50% and above, HR greater than FAR, and HSS 0.300 or higher). Overall, the Borneo OLR box did the best job in predicting cool and warm events from a

zero to five-month lead time. However, it is important to note that month-to-month comparisons can show differences in the accuracy of each predictor. It is important to consider many predictors and perform multiple hindcasts to test the accuracy of each predictor.

Table 13. Verification metrics for DJF SCS v wind hindcasts generated using tercile matching (0-5 month lead times)

0 Month Lead Time (DJF)

	Cool Events				Warm Events				Neutral Events			
Predictor Boxes	*% Correct*	*HR*	*FAR*	*HSS*	*% Correct*	*HR*	*FAR*	*HSS*	*% Correct*	*HR*	*FAR*	*HSS*
CTP SST Box	73.1%	0.588	0.412	0.388	65.4%	0.471	0.529	0.213	61.5%	0.444	0.556	0.150
Borneo OLR Box	76.9%	0.647	0.353	0.476	76.9%	0.647	0.353	0.476	61.5%	0.444	0.556	0.150
Chile OLR Box	69.2%	0.529	0.471	0.301	69.2%	0.529	0.471	0.301	61.5%	0.444	0.556	0.150
ONI	69.2%	0.529	0.471	0.301	73.1%	0.588	0.412	0.388	61.5%	0.444	0.556	0.150

1 Month Lead Time (NDJ)

	Cool Events				Warm Events				Neutral Events			
Predictor Boxes	*% Correct*	*HR*	*FAR*	*HSS*	*% Correct*	*HR*	*FAR*	*HSS*	*% Correct*	*HR*	*FAR*	*HSS*
CTP SST Box	73.1%	0.588	0.412	0.388	69.2%	0.529	0.471	0.301	65.4%	0.500	0.500	0.235
Borneo OLR Box	76.9%	0.647	0.353	0.476	69.2%	0.529	0.471	0.301	53.8%	0.333	0.667	-0.020
Chile OLR Box	73.1%	0.588	0.412	0.388	71.1%	0.529	0.438	0.334	55.8%	0.389	0.632	0.035
ONI	73.1%	0.588	0.412	0.388	73.1%	0.588	0.412	0.388	65.4%	0.500	0.500	0.235

2 Month Lead Time (OND)

	Cool Events				Warm Events				Neutral Events			
Predictor Boxes	*% Correct*	*HR*	*FAR*	*HSS*	*% Correct*	*HR*	*FAR*	*HSS*	*% Correct*	*HR*	*FAR*	*HSS*
CTP SST Box	73.1%	0.588	0.412	0.388	69.2%	0.529	0.471	0.301	65.4%	0.500	0.500	0.235
Borneo OLR Box	73.1%	0.588	0.412	0.388	69.2%	0.529	0.471	0.301	65.4%	0.500	0.500	0.235
Chile OLR Box	65.4%	0.471	0.529	0.213	73.1%	0.588	0.412	0.388	50.0%	0.278	0.722	0.150
ONI	73.1%	0.588	0.412	0.388	73.1%	0.588	0.412	0.388	69.2%	0.556	0.444	0.320

3 Month Lead Time (SON)

	Cool Events				Warm Events				Neutral Events			
Predictor Boxes	*% Correct*	*HR*	*FAR*	*HSS*	*% Correct*	*HR*	*FAR*	*HSS*	*% Correct*	*HR*	*FAR*	*HSS*
CTP SST Box	73.1%	0.588	0.412	0.388	65.4%	0.471	0.529	0.213	65.4%	0.500	0.500	0.235
Borneo OLR Box	73.1%	0.588	0.412	0.388	76.9%	0.647	0.353	0.476	61.5%	0.444	0.556	0.150
Chile OLR Box	61.5%	0.412	0.588	0.126	69.2%	0.529	0.471	0.301	53.8%	0.333	0.667	-0.020
ONI	73.1%	0.588	0.412	0.388	73.1%	0.588	0.412	0.388	73.1%	0.611	0.389	0.405

4 Month Lead Time (ASO)

	Cool Events				Warm Events				Neutral Events			
Predictor Boxes	*% Correct*	*HR*	*FAR*	*HSS*	*% Correct*	*HR*	*FAR*	*HSS*	*% Correct*	*HR*	*FAR*	*HSS*
CTP SST Box	69.2%	0.529	0.471	0.301	61.5%	0.412	0.588	0.126	61.5%	0.444	0.556	0.150
Borneo OLR Box	69.2%	0.529	0.471	0.301	73.1%	0.588	0.412	0.388	65.4%	0.500	0.500	0.235
Chile OLR Box	65.4%	0.470	0.529	0.213	61.5%	0.412	0.588	0.126	53.8%	0.333	0.667	-0.020
ONI	69.2%	0.529	0.471	0.301	73.1%	0.588	0.412	0.388	69.2%	0.556	0.444	0.320

5 Month Lead Time (JAS)

	Cool Events				Warm Events				Neutral Events			
Predictor Boxes	*% Correct*	*HR*	*FAR*	*HSS*	*% Correct*	*HR*	*FAR*	*HSS*	*% Correct*	*HR*	*FAR*	*HSS*
CTP SST Box	73.1%	0.588	0.412	0.388	65.1%	0.412	0.588	0.126	65.4%	0.500	0.500	0.235
Borneo OLR Box	76.9%	0.647	0.353	0.476	69.2%	0.529	0.471	0.301	57.7%	0.389	0.611	0.065
Chile OLR Box	69.2%	0.529	0.471	0.301	61.5%	0.412	0.588	0.126	57.7%	0.389	0.611	0.065
ONI	69.2%	0.529	0.471	0.301	69.2%	0.529	0.471	0.301	65.4%	0.500	0.500	0.235

The four predictors used to create the predictions are listed in the left column. Explanations for the metrics presented in this table can be found in Chapter II Section C.4

G. LINEAR REGRESSION HINDCASTING

After we performed and scored the hindcasts for our top four predictors using tercile matching, we performed LR on the same top four predictors to determine if the LR method serves as a better LRF method. The R^2 and p-values (which are discussed in Chapter II Section C.5) for each individual predictor are listed in Table 14. Up through the five-month lead, all predictors maintain p-values below our .05 threshold, which is a sign that the relationships between our predictors and DJF SCS v winds are statistically significant. At the five-month lead, the Chile OLR box p-value was 0.025, which was the highest p-value for any single predictor at any lead time. The Chile OLR box also showed the highest p-values when compared to the other three predictors through the zero to five-month period. However, we deemed the Chile OLR correlations and tercile matching results sufficient to use Chile OLR in our LR modeling. Furthermore, since the CTP SST box and ONI essentially capture the same area of the equatorial Pacific and ONI showed slightly better p-values, we decided to use just ONI for our SLR and MLR models.

In summary, for our LR results, we will discuss SLR models using Borneo OLR, Chile OLR, and ONI independently and MLR models with combinations of Borneo OLR, Chile OLR, and ONI. There are limitless numbers of single and multiple predictors that could potentially provide the best LRF. We encourage future researchers to continue finding additional predictors and combinations. We will discuss this later in Chapter IV Section B.

Table 14. R2 and p-values for our top four predictors

0 Month Lead (DJF)		
Predictor	**R^2**	**p-value**
CTP SST Box	0.314	1.57E-05
Borneo OLR Box	0.504	3.70E-09
Chile OLR Box	0.258	1.23E-04
ONI (SST)	0.335	6.88E-06
1 Month Lead (NDJ)		
Predictor	**R^2**	**p-value**
CTP SST Box	0.322	1.16E-05
Borneo OLR Box	0.422	1.89E-07
Chile OLR Box	0.293	3.46E-05
ONI (SST)	0.322	1.16E-05
2 Month Lead (OND)		
Predictor	**R^2**	**p-value**
CTP SST Box	0.321	1.21E-05
Borneo OLR Box	0.326	9.74E-06
Chile OLR Box	0.254	1.37E-04
ONI (SST)	0.315	1.48E-05
3 Month Lead (SON)		
Predictor	**R^2**	**p-value**
CTP SST Box	0.296	3.10E-05
Borneo OLR Box	0.325	1.04E-05
Chile OLR Box	0.216	5.13E-04
ONI (SST)	0.302	2.46E-05
4 Month Lead (ASO)		
Predictor	**R^2**	**p-value**
CTP SST Box	0.271	7.63E-05
Borneo OLR Box	0.318	1.33E-05
Chile OLR Box	0.156	3.80E-03
ONI (SST)	0.285	4.61E-05
5 Month Lead (JAS)		
Predictor	**R^2**	**p-value**
CTP SST Box	0.247	1.79E-04
Borneo OLR Box	0.295	3.14E-05
Chile OLR Box	0.097	0.025
ONI (SST)	0.274	6.83E-05

These values were obtained by running a linear regression between our top four predictors (left column) and the DJF SCS v winds. We show results from a zero-month lead time to a five-month lead time.

As with our tercile matching method, our goal for LR was to predict the tercile of the DJF SCS v winds from a zero to five-month time lead. Verification metrics for our SLR models are summarized in Table 15. These results were very similar to the tercile matching verification results shown in Table 13. This indicates that, although somewhat rudimentary, the tercile matching method can serve as a useful LRF tool for single predictors and performs close to a SLR model. However, these SLR models are not the best LR results to compare to the tercile matching results. Because of this, we will only compare our cross validated MLR scores with our tercile matching scores.

Table 15. Verification metrics for DJF SCS v wind hindcasts generated using simple linear regression (0-5 month lead times)

0 Month Lead Time (DJF)

	Cool Events				Warm Events				Neutral Events			
Predictor Boxes	*% Correct*	*HR*	*FAR*	*HSS*	*% Correct*	*HR*	*FAR*	*HSS*	*% Correct*	*HR*	*FAR*	*HSS*
Borneo OLR Box	73.1%	0.588	0.412	0.388	65.4%	0.471	0.529	0.213	61.5%	0.444	0.556	0.150
Chile OLR Box	69.2%	0.529	0.471	0.301	69.2%	0.529	0.471	0.301	61.5%	0.444	0.556	0.150
ONI	73.1%	0.588	0.412	0.388	65.4%	0.471	0.529	0.213	61.5%	0.444	0.556	0.150

1 Month Lead Time (NDJ)

	Cool Events				Warm Events				Neutral Events			
Predictor Boxes	*% Correct*	*HR*	*FAR*	*HSS*	*% Correct*	*HR*	*FAR*	*HSS*	*% Correct*	*HR*	*FAR*	*HSS*
Borneo OLR Box	76.9%	0.647	0.353	0.476	69.2%	0.529	0.471	0.301	53.8%	0.333	0.667	-0.020
Chile OLR Box	73.1%	0.588	0.412	0.388	69.2%	0.529	0.471	0.301	53.8%	0.333	0.667	-0.020
ONI	73.1%	0.588	0.412	0.388	73.1%	0.588	0.412	0.388	65.4%	0.500	0.500	0.235

2 Month Lead Time (OND)

	Cool Events				Warm Events				Neutral Events			
Predictor Boxes	*% Correct*	*HR*	*FAR*	*HSS*	*% Correct*	*HR*	*FAR*	*HSS*	*% Correct*	*HR*	*FAR*	*HSS*
Borneo OLR Box	73.1%	0.588	0.412	0.388	69.2%	0.529	0.471	0.301	65.4%	0.500	0.500	0.235
Chile OLR Box	65.4%	0.471	0.529	0.213	73.1%	0.588	0.412	0.388	50.0%	0.278	0.722	-0.105
ONI	73.1%	0.588	0.412	0.388	73.1%	0.588	0.412	0.388	69.2%	0.556	0.444	0.320

3 Month Lead Time (SON)

	Cool Events				Warm Events				Neutral Events			
Predictor Boxes	*% Correct*	*HR*	*FAR*	*HSS*	*% Correct*	*HR*	*FAR*	*HSS*	*% Correct*	*HR*	*FAR*	*HSS*
Borneo OLR Box	73.1%	0.588	0.412	0.388	76.9%	0.647	0.353	0.476	61.5%	0.444	0.556	0.150
Chile OLR Box	61.5%	0.412	0.588	0.126	69.2%	0.529	0.471	0.301	53.8%	0.333	0.667	-0.020
ONI	73.1%	0.588	0.412	0.388	73.1%	0.588	0.412	0.388	73.1%	0.611	0.389	0.405

4 Month Lead Time (ASO)

	Cool Events				Warm Events				Neutral Events			
Predictor Boxes	*% Correct*	*HR*	*FAR*	*HSS*	*% Correct*	*HR*	*FAR*	*HSS*	*% Correct*	*HR*	*FAR*	*HSS*
Borneo OLR Box	69.2%	0.529	0.471	0.301	73.1%	0.588	0.412	0.388	65.4%	0.500	0.500	0.235
Chile OLR Box	65.4%	0.471	0.529	0.213	61.5%	0.411	0.588	0.126	53.8%	0.333	0.667	-0.020
ONI	69.2%	0.529	0.471	0.301	73.1%	0.588	0.412	0.388	69.2%	0.556	0.444	0.320

5 Month Lead Time (JAS)

	Cool Events				Warm Events				Neutral Events			
Predictor Boxes	*% Correct*	*HR*	*FAR*	*HSS*	*% Correct*	*HR*	*FAR*	*HSS*	*% Correct*	*HR*	*FAR*	*HSS*
Borneo OLR Box	76.9%	0.647	0.353	0.476	69.2%	0.529	0.471	0.301	57.7%	0.389	0.611	0.065
Chile OLR Box	69.2%	0.529	0.471	0.301	61.5%	0.411	0.588	0.126	57.7%	0.389	0.611	0.065
ONI	69.2%	0.529	0.471	0.301	69.2%	0.529	0.471	0.301	65.4%	0.500	0.500	0.235

Hindcasts were created using the predictors listed in the left column.

We next created three MLR models consisting of ONI, Borneo OLR box, and Chile OLR box predictors. The three combinations were: (1) ONI, Borneo OLR, and Chile OLR; (2) ONI and Borneo OLR; and (3) ONI and Chile OLR. We decided to use ONI in all three combinations due to its high correlation with the DJF SCS v winds and the high R^2/low p-values we found in Table 14.

We first calculated the R^2 and p-values for the new combinations. These results can be found in Table 16. We found that when all three predictors (ONI, Borneo OLR, and Chile OLR) were combined, at least one of the predictors had a p-value well above our benchmark of 0.05. These high p-values indicate that these combinations of all three predictors are problematic. For the ONI/Borneo OLR combination, we found that the p-values at zero to one month lead times for ONI were quite high. However, the ONI p-values decrease at longer lead times. For this reason, we will only consider hindcasts for two to five-month lead times with this combination of ONI and Borneo OLR. For the ONI/Chile OLR combination, we found that their R^2 values were lower than the R^2 values for the ONI/Borneo OLR combination.

We did cross validated hindcastings for all three combinations, even though some predictors showed high p-values when combined with another predictor. However, in this section, we will only discuss the results from the ONI/Borneo OLR combination from a two to five-month lead time. The cross validated hindcasts for the ONI/Borneo OLR/Chile OLR and ONI/Chile OLR can be found in the appendix.

Table 16. R2 and p-values for combinations of ONI, Borneo OLR, and Chile OLR

0 Month Lead (DJF)				
Predictor	R^2	p-value		
		ONI	Borneo OLR	Chile OLR
ONI/Borneo OLR/Chile OLR	0.511	0.912	3.17E-04	0.518
ONI/Borneo OLR	0.506	0.674	1.46E-04	-
ONI/Chile OLR	0.357	8.29E-03	-	0.205
1 Month Lead (NDJ)				
Predictor	R^2	p-value		
		ONI	Borneo OLR	Chile OLR
ONI/Borneo OLR/Chile OLR	0.466	0.448	0.00666	0.164
ONI/Borneo OLR	0.444	0.172	1.93E-03	-
ONI/Chile OLR	0.376	0.013	-	0.043
2 Month Lead (OND)				
Predictor	R^2	p-value		
		ONI	Borneo OLR	Chile OLR
ONI/Borneo OLR/Chile OLR	0.406	0.346	0.054	0.089
ONI/Borneo OLR	0.369	0.074	0.046	-
ONI/Chile OLR	0.358	0.007	-	0.076
3 Month Lead (SON)				
Predictor	R^2	p-value		
		ONI	Borneo OLR	Chile OLR
ONI/Borneo OLR/Chile OLR	0.370	0.238	0.040	0.140
ONI/Borneo OLR	0.368	0.072	0.028	-
ONI/Chile OLR	0.340	0.004	-	0.097
4 Month Lead (ASO)				
Predictor	R^2	p-value		
		ONI	Borneo OLR	Chile OLR
ONI/Borneo OLR/Chile OLR	0.360	0.164	0.028	0.705
ONI/Borneo OLR	0.359	0.086	0.022	-
ONI/Chile OLR	0.292	0.004	-	0.489
5 Month Lead (JAS)				
Predictor	R^2	p-value		
		ONI	Borneo OLR	Chile OLR
ONI/Borneo OLR/Chile OLR	0.383	0.013	0.005	0.416
ONI/Borneo OLR	0.375	0.016	0.007	-
ONI/Chile OLR	0.274	0.001	-	0.967

The results of the hindcasts for our ONI/Borneo OLR MLR model can be found in Table 17. We found that our MLR hindcasts of DJF cool and warm events from a two to five-month lead satisfied our scoring benchmarks of PC greater than 0.5, HR equal to or greater than FAR, and HSS 0.300 or greater. However, we did not see a considerable increase in skill over tercile matching scores. The highest scoring metrics for DJF cool events with our MLR models were our five-month lead time of JAS. These scores, however, did not beat the JAS scores for the single Borneo OLR box we used in tercile matching. The highest scoring metrics for DJF warm events was our four-month lead time of ASO. The scores of PC of 76.9%, HR of 0.647, FAR of 0.353, and HSS of 0.476 were

higher than our tercile matching models. The scoring metrics at two to three-months for our combined MLR were at or below the metrics for tercile matching.

Table 17. Verification metrics for DJF SCS v wind hindcasts generated using multiple linear regression (2-5 month lead times)

2 Month Lead Time (OND)												
	Cool Events				Warm Events				Neutral Events			
Predictor	*% Correct*	*HR*	*FAR*	*HSS*	*% Correct*	*HR*	*FAR*	*HSS*	*% Correct*	*HR*	*FAR*	*HSS*
ONI/Borneo OLR	69.2%	0.529	0.471	0.301	69.2%	0.529	0.471	0.301	61.5%	0.444	0.556	0.150
3 Month Lead Time (SON)												
	Cool Events				Warm Events				Neutral Events			
Predictor	*% Correct*	*HR*	*FAR*	*HSS*	*% Correct*	*HR*	*FAR*	*HSS*	*% Correct*	*HR*	*FAR*	*HSS*
ONI/Borneo OLR	73.1%	0.588	0.412	0.388	69.2%	0.529	0.471	0.301	69.2%	0.556	0.444	0.321
4 Month Lead Time (ASO)												
	Cool Events				Warm Events				Neutral Events			
Predictor	*% Correct*	*HR*	*FAR*	*HSS*	*% Correct*	*HR*	*FAR*	*HSS*	*% Correct*	*HR*	*FAR*	*HSS*
ONI/Borneo OLR	73.1%	0.588	0.412	0.388	76.9%	0.647	0.353	0.476	65.4%	0.500	0.500	0.235
5 Month Lead Time (JAS)												
	Cool Events				Warm Events				Neutral Events			
Predictor	*% Correct*	*HR*	*FAR*	*HSS*	*% Correct*	*HR*	*FAR*	*HSS*	*% Correct*	*HR*	*FAR*	*HSS*
ONI/Borneo OLR	76.9%	0.647	0.353	0.476	69.2%	0.529	0.471	0.301	65.4%	0.500	0.500	0.235

Hindcasts were created using the predictors listed in the left column.

H. COMPARING OUR TERCILE MATCHING AND LINEAR REGRESSION MODELS

We found that the hindcast results using both the tercile matching method and MLR method show skill at long lead times. As such, both methods can be useful in the operational forecasting of DJF SCS v wind anomalies. Most importantly, both tercile matching and MLR skill scores are similar at longer leads. However, on average, the MLR hindcasts tend to have lower FAR values than the average FAR scores for tercile matching. At shorter leads, tercile matching scores tend to be better overall than MLR scores. It is important to note that the tercile matching results vary by the predictor, lead time, and skill score. For example, Borneo OLR may be the best predictor at one lead time, but ONI shows slightly better skill scores at the another lead time. The differences from month to month and predictor to predictor make it difficult to use tercile matching as an operational forecasting method. With our MLR method, the predictors would be the same for lead times of two to five months. For these reasons, we believe that our MLR method of

combining predictors may be easier to employ in operational forecasting. Both our tercile matching and MLR methods show skill at subseasonal to seasonal lead times. However, additional research into potential predictors and combinations of predictors would likely lead to better skill scores.

We also produced experimental forecasts of SCS v winds for DJF 2021–2022. We did this to test the potential operational use of our tercile matching and MLR forecasting methods. We used predictor data from JAS, ASO, and SON of 2021. We again used 52 years (1970-2021 vice 1969–2020) to help make our prediction, so the terciles were still 17 AN, 17 BN, and 18 NN years. For the tercile matching method, we used the Borneo OLR box since the hindcasts using this predictor received the highest scores at the ASO, JAS, and SON lead times out of our four single predictors. For the MLR method, we used the ONI and Borneo OLR combination. Our results are summarized in Table 18. We found that both methods were very consistent in predicting BN conditions, and thus a cool event, in the SCS in DJF 2021–2022, at all lead times (the JAS, ASO, and SON lead times). Table 18 also shows, for each lead time, the probability of occurrence of BN conditions in DJF 2021–2022. We calculated this probability using the method described in Heidt (2009) and the hindcast results for predicting BN events in DJF 1970–2021 using our tercile matching model with the Borneo OLR predictor and our MLR model with the ONI and Borneo OLR predictors. Note that the highest probability of forecasting a cool event occurs at the longest lead time (JAS) for both forecasting methods but remains above 50% for both models at all lead times. For comparison, note that the normal probability of BN events is 33%, so we are predicting a substantially greater than normal chance of a BN (cool) event in the SCS in DJF 2021–2022 (20-32% greater than the normal probability).

Table 18. Summary of 2021–2022 DJF SCS v wind forecast using tercile matching and multiple linear regression models

Forecast for 2021-2022 DJF SCS v winds				
	Tercile Matching Model (Borneo OLR)		MLR Model (ONI/Borneo OLR)	
Lead time	Tercile	Probability	Tercile	Probability
JAS	BN (cool event)	65%	BN (cool event)	65%
ASO	BN (cool event)	53%	BN (cool event)	59%
SON	BN (cool event)	59%	BN (cool event)	59%

I. CLIMATE CHANGE IMPACTS ON COOL AND WARM EVENTS

After we conducted our hindcasts, we wanted to determine how climate change has affected the strength and frequency of cool and warm events from 1970–2021. Our first step was the reanalyze our initial SCS DJF 1000 mb v wind time series (Figure 7 and Figure 8). Figure 37 breaks up our SCS DJF 1000 mb v winds into two time periods to analyze the changes over 1970–2021. The first period encompasses 21 years from 1970–1991 and the second section encompasses 21 years from 2001–2021. Overall, the strength of the SCS v winds has decreased over the 52-year period from 1970–2021, as indicated by the slope of the trendline (black dashed line). To quantify the amount of decrease, we calculated a negative (-)5.7% percent change from 1970–2021, meaning the northerly v wind speeds have decreased by about 5.7% over the last 52 years.

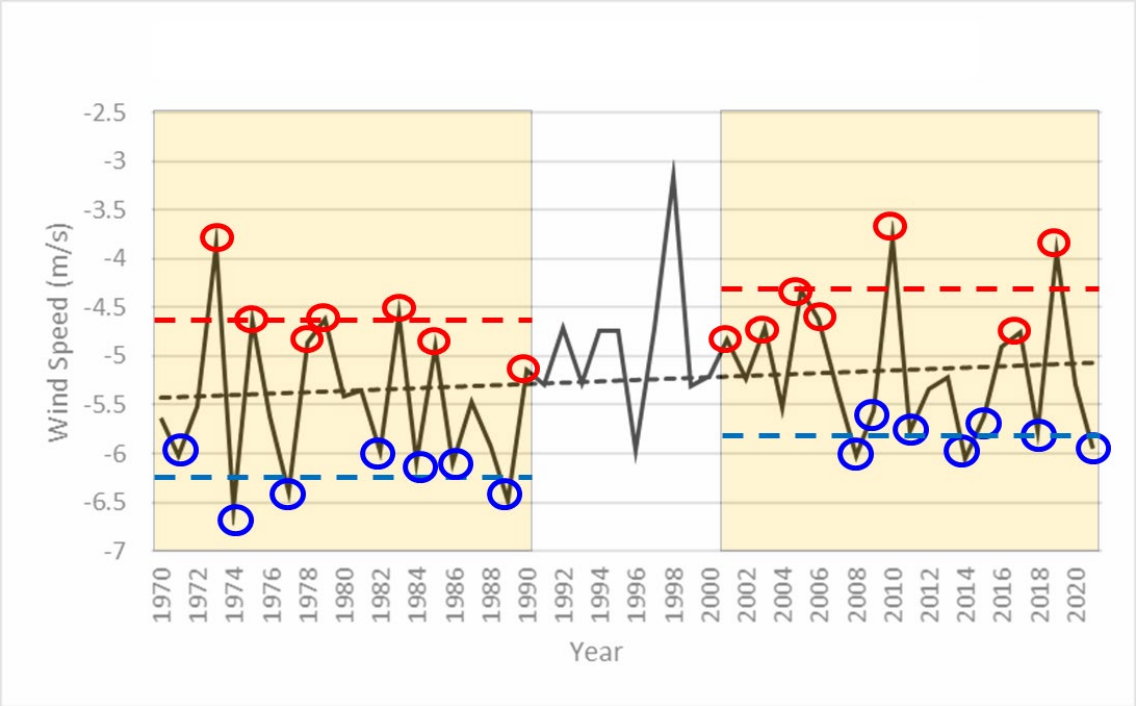

The red circles denote warm events and blue circles denote cool events. The red dashed lines are the 21 year averages of warm events. The blue dashed lines are the 21 year averages of cool events. The black dashed line is the trendline over the entire period from 1970–2021.

Figure 37. Chunk analysis of SCS DJF 1000 mb v winds from 1970–2021

Next, we analyzed the two 21-year periods separately. Within each 21 year period, we separated the years into cool events, warm events, and neutral events. By using 21 years, we were able to divide into three groups of 7 years for each category. The years used for this analysis can be found in Table 19.

Table 19. Chunk analysis cool and warm events

DJF			
1970-1990		2001-2021	
Cool	Warm	Cool	Warm
1971	1973	2008	2001
1974	1975	2009	2003
1977	1978	2011	2005
1982	1979	2014	2006
1986	1983	2015	2010
1988	1985	2018	2017
1989	1990	2021	2019

The average v wind speed for cool events during the first 21-year period was about -6.25 m/s compared to -5.8 m/s for the most recent 21-year period. The difference between periods is a positive 0.45 m/s, or in other words, there is a 0.45 m/s decrease in northerly v wind speed. This indicates that cool events are less extreme today than in the past. Meanwhile, the average v wind speed for warm events during the first 21-year period was about -4.65 m/s compared to -4.42 m/s for the most recent 21-year period. Like the cool events, this difference of positive 0.23 m/s indicates that warm events are less extreme today than in the past. However, the wind speed changes for cool events are nearly double that of warm events. To help identify the factors behind the changes over our 52-year period, we performed a multidecadal analysis of various climate variables.

1. SLP Multidecadal Analysis

We created an SLP composite difference plot (Figure 38) using the most recent 21-year period (2001-2021) minus the first 21 year period (1970-1990). To understand the composite difference plot, we needed to compare the difference plot with our original

SLPA analysis for cool and warm events (Figure 13). For reference, for cool (warm) events, we found positive (negative) SLPAs along the China coastline and negative (positive) SLPAs over the MC. Our difference composite shows a broad area of negative difference SLP values along the China coastline and over the MC, indicating the pressure gradient between the China coastline and the MC has weakened over our 52-year period. Essentially, this indicates that the strength of both cool and warm events has decreased from 1970 to 2021. We also showed that the inferred wind difference (black arrow) opposes the mean winds from the north during DJF, which is consistent with the change in SLP over the past 52 years.

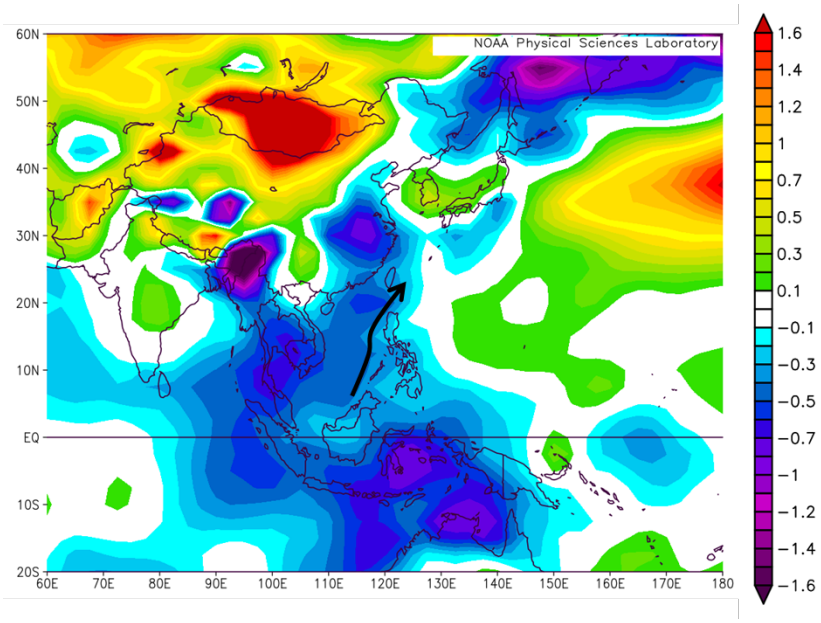

The black arrow represents the inferred wind difference based on SLP differences. The south to north direction opposes, or weakens, the predominant northerly flow. PSL based figure.

Figure 38. SLP composite difference for DJF (2001-2021 minus 1970–1990)

2. SST Multidecadal Analysis

We created Figure 40 to show the multidecadal trend from 1970–2021. There is a clear increase in SSTs in the SCS, as indicated by the black dashed trendline.

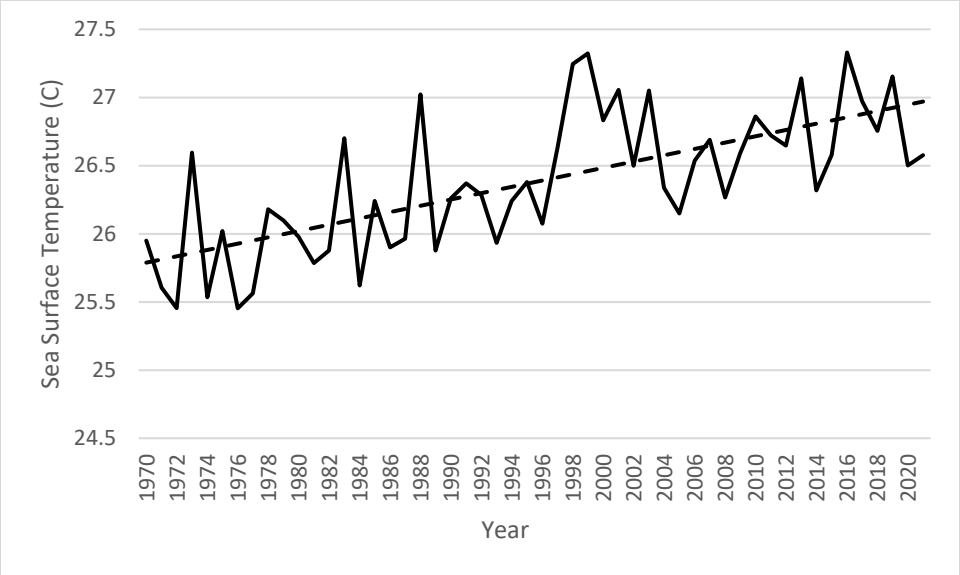

The black dashed line indicated the trend of SSTs in the SCS over our 52 year period

Figure 39. SSTs (°C) in the SCS from 1970–2021

We created Figure 40 to show the exact differences in SSTs from our first period to second period. We can see that SSTAs in the SCS and WNP have increased over the 52-year period, indicating a general warming trend. Increased SSTs throughout the region could provide a reason for the decrease in SLPs throughout the region. Increased SSTs cause increased evaporation and rising motion, which will decrease the SLPs. There will be an eventual increase in clouds and precipitation over the region as well.

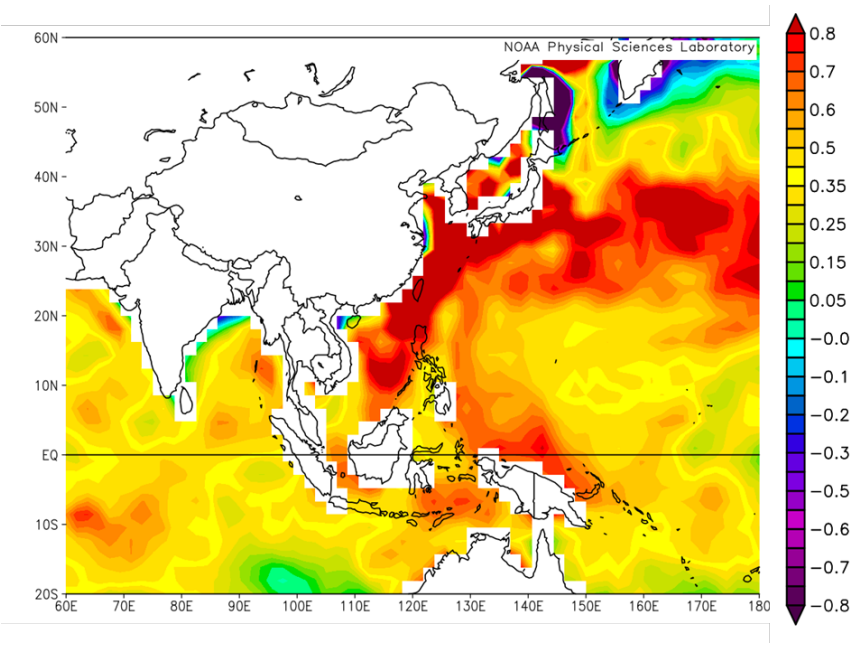

Figure 40. SST composite difference (2001–2021 minus 1970–1990) for DJF. PSL based figure.

3. Frequency of Cool and Warm Events

We created Figure 41 to determine the change in frequency of cool and warm events from 1970–2021. To generate this figure, we used the same tercile method to break the data into cool, warm, and neutral events. However, we applied this technique to each winter month (November-March). By doing so, we were able to determine how the number of cool and warm events have changed from 1970 to 2021. We found that the overall frequency of cool (warm) events has decreased (increased) from 1970–2021.

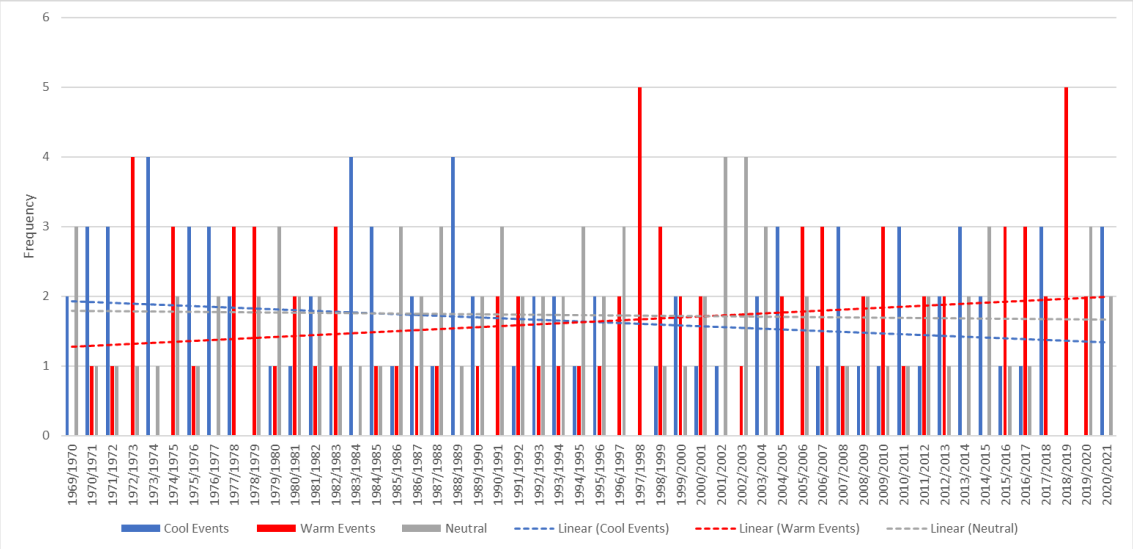

This figure shows how the number of cool (warm) events has decreased (increased) from 1970–2021

Figure 41. Frequency of cool and warm events from 1970–2021

THIS PAGE INTENTIONALLY LEFT BLANK

IV. CONCLUSIONS AND RECOMMENDATIONS

A. SUMMARY AND CONCLUSIONS

Our motivation to conduct LRF research on the winter winds in the SCS was due to: (1) the U.S. Navy's posturing, which is defined by current political tensions within the SCS region; (2) the complexity of the EAWM winds that vary on different spatial and temporal scales; and (3) the lack of a credible LRF technique that can provide useful forecasts for future anomalous wind events in the SCS.

As noted in Chapter I, we wanted to answer the following questions by the end of our research:

1. What are the large scale climate processes that drive variations in SCS meridional (v) wind intensity?
2. How do the fluctuations in SCS v wind intensity affect operationally relevant variables (waves, SLD, evaporation ducts, precip, etc)?
3. Are these variations in SCS v wind intensity predictable at S2S lead times (1 to 5 months)?
4. What indices are the best predictors for SCS v wind intensity? Do combinations of indices lead to better prediction?
5. How has climate change affected the SCS v winds and related atmospheric and oceanic variables?

Through a comprehensive analysis of multiple climate variables, we found that cool and warm events are well represented within the climate system. Generally speaking, cool and warm events show anomalies that are opposite in sign, but magnitudes of their anomalies vary in strength and locations. We were able to show the importance of the SLP differences between the China mainland and the MC, and how these differences impact the winds in the SCS. Although the EAWM is associated with the major SH system over the Asian continent, these pressure anomalies between China and MC play a major role at a location like the SCS. We also found that different regions in close proximity, like the ECS

and SCS, show differences temporary from one another. For this reason, it is important to treat each region separately and we only considered the impact on the SCS v winds.

We created schematics that summarize the effects of multiple climate variables on the SCS v winds. We connected SSTAs in the equatorial Pacific to the anomalous Rossby wave train response we found in the northern hemisphere. These schematics highlighted new findings and validated prior research on the EAWM. We found unique differences between the overall EAWM and the SCS region. We were able to conclude that equatorial SSTs are good indicators of cool and warm events in the SCS.

To provide additional useful results to the U.S. Navy operators, we utilized FNMOC's ACAF plotting tool to create composites of operationally relevant variables (SWH, SLD, EDH, cloud cover, and precipitation) that are seen during DJF cool and warm events in the SCS. We found it important to provide as much information as possible with regards to the anomalous v wind conditions. We quantified the anomalies and pointed out the locations of the highest differences from the LTM. We learned that v wind deviations from the LTM impact a wide variety of variables. In some cases, the anomalies may appear to be small and insignificant. However, depending on the naval platform, small changes from the LTM could impact the location of an operation when planned out at long lead times. For example, ISR missions may require zero cloud cover between the sensor and surface. We provided cloud cover percentages that could be expected during cool and warm events to assist planners with potential future operations.

To determine the predictability of the anomalous v wind conditions in the SCS, we used two LRF methods: tercile matching and LR. To determine which predictors we would test, we first calculated correlation coefficients between our predictand (DJF SCS v wind) and climate variables that we believed are: (1) connected to the SCS via evidence from our conditional composite results; and (2) were investigated in prior work, but lacked a LRF projection. We found that global SSTs, especially in the equatorial region, were highly correlated with the SCS v winds. We also found that OLR, which we used as an indicator of convection we found near the MC, correlated quite well with the SCS v winds at long lead times. We correlated other known climate indices, like ONI, AO, NAO, etc., that were mentioned in prior research of the EAWM to round out the list of potential predictors. We

narrowed our list of predictors down to four potential predictors: an SST region in the CTP, a OLR region over the MC, a OLR region over near Chile, and the ONI. With these four predictors, we conducted numerous hindcasts from 1970–2021 and scored the hindcasts via 2x2 contingency tables. We provided metrics to include PC, HR, FAR, and HSS to determine the validity of each forecast. For the LR method, we carefully analyzed the output statistics of the regression to include R^2 and p-value metrics. For our study, we found that when we combined our two best single predictors, ONI and the Borneo OLR box, into a MLR model, the hindcasts of DJF cool and warm events from a two to five-month lead satisfied our scoring benchmarks of PC greater than 0.5, HR equal to or greater than FAR, and HSS 0.300 or greater. However, we did not see a considerable increase in skill over tercile matching scores. Ultimately, we believe that a strong combination of predictors can successfully increase the predictability of SCS v wind at S2S lead times.

We also conducted an analysis of the effects of climate change on the DJF SCS v winds. Overall, we found that the DJF v winds in the SCS have decreased over the past 52 years. We also found that the number of cool events has decreased over the past 52 years, while the number of warm events has increased over the past 52 years.

B. FUTURE WORK

With our research, we created numerous opportunities for future research that involves the LRF of v winds in the SCS. The possibilities for additional LRF methods and techniques for SCS v winds expand well beyond the scope of our research. We highly encourage future work in this field to build upon our results and continue the quest to find the best LRF results. The following is a list of potential research topics:

1. Since our work focused on monthly values for our variables of interest, it would be beneficial to utilize daily data to conduct a study on cool and warm events in the SCS. One topic of interest could be the effects of the Madden-Julian Oscillation (MJO) on the SCS v winds. The MJO is an eastward propagating intraseasonal (1-2 month) oscillation that mostly starts in the tropical Indian Ocean (Murphree 2021b). Prior research (Jeong et al. 2005; Xavier et al. 2020) has related MJO with the EAWM.

However, it would be beneficial to focus on a smaller region, like the SCS, and determine how MJO specifically affects the SCS v winds during DJF. Focusing on MJO would require larger daily data sets and perhaps greater computing power. Jones (2021) used machine learning while working with daily data sets, and this type of computation could assist with a daily analysis of the SCS v winds.

2. Another area of future research could incorporate some of the methods used by Ilczuk (2016) to determine how MJO and ENLN interact to affect the v winds in the SCS. Since we saw such a strong correlation to ENLN, it could be useful to combine MJO and ENLN effects to increase LRF skill.

3. For our research, we found anomalies based on the currently recognized TCN, which is 1981–2010. Future work could include using an Optimal Climate Normal (OCN) approach, which involves using the most recent ten years to capture how climate change is impacting our variables. Prior research (Lemke 2010) discusses the OCN approach in his work with precipitation off the Horn of Africa. Similar techniques could be applied to the v winds in the SCS.

4. We briefly discussed FNMOC's ESPC model in Chapter I Section B. Future work could entail using ESPC model output to create hindcasts for daily/monthly averaged winds in the SCS. These hindcasts will help express the current skill level of the ESPC model and could potentially improve forecasting skill out to a few weeks.

5. There are numerous predictands that could be used to quantify the strength of the v winds in the SCS. Wang and Chen (2014) provided a list of other potential predictands for the EAWM index based on correlation coefficients. They found that a SLP index performed well in representing "[t]he thermal contrast between the Asian continent and the adjacent oceans…" (Wang and Chen 2014) and the relationship of this contrast

with the EAWM. Our study could be replicated by using a different predictand, such as SLP, to determine which predictand variable provides the best LRF skill.

6. There are numerous predictors that can either be used as a single predictor or combined with other predictors to improve the skill of the linear regression LRF technique. We believe that many other predictor combinations can be tested using the techniques explained in our research. There are also opportunities to conduct cross validation of linear regression via the "leave-one out" approach (Wilks 2006; Lemke 2010; Stone 2010).

7. There are opportunities to pursue the effects of climate change on cool and warm events in the SCS. For example, future research could involve looking at the climate variables for warm and cool events on a multidecadal scale to identify impacts on cool and warm events due to climate change.

THIS PAGE INTENTIONALLY LEFT BLANK

APPENDIX. RESULTS OF ADDITIONAL HINDCASTS

As discussed in Chapter III, Section G, we performed cross validated hindcasts for ONI/Borneo OLR/Chile OLR combination and ONI/Chile OLR combination. Table 20 summarizes our results for those two combinations of predictors.

Table 20. Multiple linear regression hindcasting results for ONI/Borneo OLR/Chile OLR and ONI/Chile OLR combinations of the DJF SCS v winds from 2–5 month time lead

2 Month Lead Time (OND)

	Cool Events				Warm Events				Neutral Events			
Predictor	*% Correct*	*HR*	*FAR*	*HSS*	*% Correct*	*HR*	*FAR*	*HSS*	*% Correct*	*HR*	*FAR*	*HSS*
ONI/Borneo OLR/Chile OLR	76.9%	0.647	0.353	0.476	73.1%	0.588	0.412	0.388	69.2%	0.556	0.444	0.320
ONI/Chile OLR	73.1%	0.588	0.412	0.388	69.2%	0.529	0.471	0.301	61.5%	0.444	0.556	0.150

3 Month Lead Time (SON)

	Cool Events				Warm Events				Neutral Events			
Predictor	*% Correct*	*HR*	*FAR*	*HSS*	*% Correct*	*HR*	*FAR*	*HSS*	*% Correct*	*HR*	*FAR*	*HSS*
ONI/Borneo OLR/Chile OLR	73.1%	0.588	0.412	0.388	69.2%	0.529	0.471	0.301	73.1%	0.611	0.389	0.405
ONI/Chile OLR	73.1%	0.588	0.412	0.388	69.2%	0.529	0.471	0.301	61.5%	0.444	0.556	0.150

4 Month Lead Time (ASO)

	Cool Events				Warm Events				Neutral Events			
Predictor	*% Correct*	*HR*	*FAR*	*HSS*	*% Correct*	*HR*	*FAR*	*HSS*	*% Correct*	*HR*	*FAR*	*HSS*
ONI/Borneo OLR/Chile OLR	69.2%	0.529	0.471	0.301	69.2%	0.529	0.471	0.301	61.5%	0.444	0.556	0.150
ONI/Chile OLR	69.2%	0.529	0.471	0.301	69.2%	0.529	0.471	0.301	65.4%	0.500	0.500	0.235

5 Month Lead Time (JAS)

	Cool Events				Warm Events				Neutral Events			
Predictor	*% Correct*	*HR*	*FAR*	*HSS*	*% Correct*	*HR*	*FAR*	*HSS*	*% Correct*	*HR*	*FAR*	*HSS*
ONI/Borneo OLR/Chile OLR	73.1%	0.588	0.412	0.388	73.1%	0.588	0.412	0.388	61.5%	0.444	0.556	0.150
ONI/Chile OLR	73.1%	0.588	0.412	0.388	73.1%	0.588	0.412	0.388	61.5%	0.444	0.556	0.150

THIS PAGE INTENTIONALLY LEFT BLANK

LIST OF REFERENCES

Annamalai, H., P. Liu, and S.-P. Xie, 2005: Southwest Indian Ocean SST variability: Its local effect and remote influence on Asian monsoons. *Journal of Climate*, **18**, 4150–4167, https://doi.org/10.1175/JCLI3533.1.

Bjerknes, J., 1969: Atmospheric teleconnections from the equatorial Pacific. *Monthly Weather Review*, **97**, 3, 163–172.

Byrne, K. L., 2018: Subseasonal to seasonal forecasting of ocean acoustic conditions: The potential for shipboard forecasting. M.S. thesis, Dept. of Meteorology, Naval Postgraduate School, 89 pp.

Chan, J. C. L., and C. Li, 2004: The East Asia Winter Monsoon. *World Scientific Series on Asia-Pacific Weather and Climate*, Chih-pei-Chang, World Scientific Publishing Company, 54–106.

Chang, C.-P., and K. M. Lau, 1979: Northeasterly cold surges and near-equatorial disturbances over the winter MONEX area during December 1974. Part II: planetary-scale aspects. *Monthly Weather Review*, **108**, 298–312.

Chang, C.-P., J. E. Erickson, and K. M. Lau, 1979: Northeasterly cold surges and near-equatorial disturbances over the winter MONEX area during December 1974. Part I: synoptic aspects. *Monthly Weather Review*, **107**, 812–829.

Chen, D., J. Sun, and Y. Gao, 2020: Effects of AO on the interdecadal oscillating relationship between the ENSO and East Asian winter monsoon. *Int J Climatol*, **40**, 4374–4383, https://doi.org/10.1002/joc.6459.

Chen, T.-C., W.-R. Huang, and J.-H. Yoon, 2004: Interannual variation of the east Asian cold surge activity. *Journal of Climate*, **17**, 401–413.

Chen, Z., R. Wu, and W. Chen, 2014: Distinguishing interannual variations of the northern and southern modes of the east Asian winter monsoon. *Journal of Climate*, **27**, 835–851, https://doi.org/10.1175/JCLI-D-13-00314.1.

CNN, 2021: Two U.S. Navy aircraft carriers conduct South China Sea drills. Accessed on 15 July 2021, https://www.cnn.com/2021/02/09/asia/us-navy-two-aircraft-carriers-south-china-sea-ml/index.html.

Council on Foreign Relations, 2021: Territorial disputes in the South China Sea. Accessed on 15 July 2021, https://cfr.org/global-conflict-tracker/conflict/territorial-disputes-south-china-sea.

China Power Project, 2017: How much trade transits the South China Sea? Accessed on 15 July 2021, https://chinapower.csis.org/much-trade-transits-south-china-sea/

Fleet Numerical Meteorology and Oceanography Center (FNMOC), 2017: ACAF Data Set Documentation. Accessed on 15 July 2021, https://portal-alpha.fnmoc.navy.mil/acaf/doc/documentation/ACAF_Dataset_Documentation_V8_29nov17.pdf

Ford, B., 2000: El Nino and La Nina effects on tropical cyclones: The mechanisms. M.S. thesis, Dept. of Meteorology, Naval Postgraduate School, 201 pp.

Gong, D.-Y., S.-W. Wang, and J.-H. Zhu, 2001: East Asian winter monsoon and Arctic Oscillation. *Geophysical Research Letters*, **28**, 2073–2076, https://doi.org/10.1029/2000GL012311.

He, S., and H. Wang, 2013: Oscillating relationship between the east Asian winter monsoon and ENSO. *Journal of Climate*, **26**, 9819–9838, https://doi.org/10.1175/JCLI-D-13-00174.1.

He, S., Y. Gao, F. Li, H. Wang, and Y. He, 2017: Impact of Arctic Oscillation on the East Asian climate: A review. *Earth-Science Reviews*, **164**, 48–62, https://doi.org/10.1016/j.earscirev.2016.10.014.

Heidt, S. L., 2009: Long-range atmosphere-ocean forecasting in support of undersea warfare operations in the western north Pacific. M.S. thesis, Dept. of Meteorology, Naval Postgraduate School, 100 pp.

Ilczuk Jr, R. E., 2016: The impacts of multiple simultaneous climate variations. M.S. thesis, Dept. of Meteorology, Naval Postgraduate School, 196 pp.

Jeong, J.-H., C.-H. Ho, B.-M. Kim, and W.-T. Kwon, 2005: Influence of the Madden-Julian Oscillation on wintertime surface air temperature and cold surges in east Asia. *J. Geophys. Res.*, **110**, 1–7, https://doi.org/10.1029/2004JD005408.

Jiang, X., S. Yang, Y. Li, A. Kumar, W. Wang, and Z. Gao, 2013: Dynamical prediction of the east Asian winter monsoon by the NCEP climate forecast system. *J. Geophys. Res. Atmos.*, **118**, 1312–1328, https://doi.org/10.1002/jgrd.50193.

Jones, K. T., 2021: Wildfire-favorable offshore wind events in California: Global-scale climate teleconnections to extreme weather and potential subseasonal to seasonal predictability. Ph.D. dissertation, Naval Postgraduate School, 170 pp.

Kalnay, E., and Coauthors, 1996: The NCEP/NCAR 40-year reanalysis project. *Bulletin of the American Meteorological Society*, **77**, 437–471.

Kim, J.-W., S.-W. Yeh, and E.-C. Chang, 2014: Combined effect of El Niño-Southern Oscillation and Pacific Decadal Oscillation on the east Asian winter monsoon. *Clim Dyn*, **42**, 957–971, https://doi.org/10.1007/s00382-013-1730-z.

Kistler, R., and Coauthors, 2001: The NCEP-NCAR 50-year reanalysis: Monthly means CD-ROM and documentation. *Bulletin of the American Meteorological Society*, **82**, 247–267.

Kohlman, K., S. Madden, T. Murphree, 2021: Marine heat waves in the eastern North Pacific: Characteristics and causes. National Oceanic and Atmospheric Administration National Weather Service *Science and Technology Infusion Climate Bulletin*, **13**, 120–125.

Lemke, B. D., 2010: Long-range forecasting in support of operations in the Horn of Africa. M.S. thesis, Dept. of Meteorology, Naval Postgraduate School, 156 pp.

Li, Q., S. Yang, T. Wu, and X. Liu, 2017: Subseasonal dynamical prediction of east Asian cold surges. *Weather and Forecasting*, **32**, 1675–1694, https://doi.org/10.1175/WAF-D-16-0209.1.

Livezey, R. E., and W. Y. Chen, 1983: Statistical field significance and its determination by Monte Carlo Techniques. *Monthly Weather Review*, **111**, 46–59.

Mattis, J., 2018: *National Defense Strategy*. Arlington, VA: Department of Defense.

McKeon, B. D., 2013: Climate analysis of evaporation ducts in the South China Sea. M.S. thesis, Dept. of Meteorology, Naval Postgraduate School, 112 pp.

Murphree, T., 2021a: Module 5: Introduction to Climate Science. Course notes, Modern Climatology (MR3610), Summer 2021.

Murphree, T., 2021b: Module 19: Madden-Julien Oscillations Part 1. Course notes, Modern Climatology (MR3610), Summer 2021.

Nitta, T., 1987: Convective activities in the tropical western Pacific and their impact on the northern hemisphere summer circulation. *Journal of the Meteorological Society of Japan. Ser. II*, **65**, 373–390.

NOAA Climate Prediction Center (CPC), 2021a: Arctic Oscillation (AO). Accessed on 05 October 2021, https://www.cpc.ncep.noaa.gov/products/precip/CWlink/daily_ao_index/ao.shtml.

NOAA Climate Prediction Center (CPC), 2021b: Cold & Warm Episodes by Season. Accessed on 15 July 2021, https://origin.cpc.ncep.noaa.gov/products/analysis_monitoring/ensostuff/ONI_v5.php

Office of the Secretary of Defense, 2017: Annual Report to Congress: Military and Security Developments Involving the People's Republic of China 2017.

Park, T.-W., C.-H. Ho, and S. Yang, 2011: Relationship between the Arctic Oscillation and cold surges over east Asia. *Journal of Climate*, **24**, 68–83, https://doi.org/10.1175/2010JCLI3529.1.

Ramsaur, D., 2009: Climate analysis and long range forecasting of radar performance in the western north Pacific. M.S. thesis, Dept. of Meteorology, Naval Postgraduate School, 116 pp.

Saha, S., and Coauthors, 2010: The NCEP climate forecast system reanalysis. *Bull. Amer. Meteor. Soc.*, **91**, 1015–1058, https://doi.org/10.1175/2010BAMS3001.1.

Schwing, F. B., T. Murphree, and P. M. Green, 2002: The Northern Oscillation Index (NOI): A new climate index for the northeast Pacific. *Progress in Oceanography*, **53**, 115–139, https://doi.org/10.1016/S0079-6611(02)00027-7.

Stone, M. M., 2010: Long-range forecasting of Arctic sea ice. M.S. thesis, Dept. of Meteorology, Naval Postgraduate School, 118 pp.

Swail, V. R., V. J. Cardone, M. Ferguson, D. J. Gummer, E. L. Harris, E. A. Orelup, and A. T. Cox, 2006: The MSC50 wind and wave reanalysis. *9th International Workshop on Wave Hindcasting and Forecasting*, Victoria B.C. Canada.

Tian, B., and K. Fan, 2020: Different prediction skill for the east Asian winter monsoon in the early and late winter season. *Clim Dyn*, **54**, 1523–1538, https://doi.org/10.1007/s00382-019-05068-6.

U.S. Naval Research Laboratory (NRL), 2021: Navy Forecasting Provides 45-day Advanced Environmental Predictions. Accessed on 16 July 2021, https://www.nrl.navy.mil/Media/News/Article/2602782/navy-forecasting-provides-45-day-advanced-environmental-predictions/.

USNI, 2018: U.S. Warship Sails Past Disputed South China Sea Artificial Island in Freedom of Navigation Mission. Accessed on 15 July 2021, https://news.usni.org/2018/03/23/u-s-warship-sails-past-disputed-south-china-sea-artificial-island-freedom-navigation-mission.

Vines, G. M., 2017: Long-range forecasting of the onset of southwest monsoon winds and waves near the Horn of Africa. M.S. thesis, Dept. of Meteorology, Naval Postgraduate School, 60 pp.

Wang, B., 2007: *The Asian Monsoon*. Springer, 787 pp.

Wang, B., R. Wu, and X. Fu, 2000: Pacific–east Asian teleconnection: How does ENSO affect east Asian climate? *Journal of Climate*, **13**, 1517–1536.

Wang, L., and W. Chen, 2014: An intensity index for the east Asian winter monsoon. *Journal of Climate*, **27**, 2361–2374, https://doi.org/10.1175/JCLI-D-13-00086.1.

Wen, C., H.-F. Graf, and H. Ronghui, 2000: The interannual variability of east Asian winter monsoon and its relation to the summer monsoon. *Adv. Atmos. Sci.*, **17**, 48–60, https://doi.org/10.1007/s00376-000-0042-5.

Wilks, D. S., 2006: *Statistical methods in the atmospheric sciences*. 2nd ed. Academic Press, 627 pp.

Xavier, P., and Coauthors, 2020: Seasonal dependence of cold surges and their interaction with the Madden–Julian Oscillation over southeast Asia. *Journal of Climate*, **33**, 2467–2482, https://doi.org/10.1175/JCLI-D-19-0048.1.

Zhang, R., A. Sumi, and M. Kimoto, 1996: Impact of El Niño on the east Asian monsoon: A diagnostic study of the '86/87 and '91/92 events. *Journal of the Meteorological Society of Japan*, **74**, 49–62, https://doi.org/10.2151/jmsj1965.74.1_49.

Zhang, Y., K. R. Sperber, and J. S. Boyle, 1997: Climatology and interannual variation of the east Asian winter monsoon: results from the 1979–95 NCEP/NCAR reanalysis. *Monthly Weather Review*, **125**, 2605–2619.

THIS PAGE INTENTIONALLY LEFT BLANK

INITIAL DISTRIBUTION LIST

1. Defense Technical Information Center
   Ft. Belvoir, Virginia

2. Dudley Knox Library
   Naval Postgraduate School
   Monterey, California